International Journal of
Molecular Sciences

MDPI

Article

Interactions between Membrane Resistance, GABA-A Receptor Properties, Bicarbonate Dynamics and Cl^--Transport Shape Activity-Dependent Changes of Intracellular Cl^- Concentration

Aniello Lombardi [1], Peter Jedlicka [2,3,4], Heiko J. Luhmann [1] and Werner Kilb [1,*]

1 Institute of Physiology, University Medical Center Mainz, Johannes Gutenberg University, Duesbergweg 6, 55128 Mainz, Germany; alombard@uni-mainz.de (A.L.); luhmann@uni-mainz.de (H.J.L.)
2 ICAR3R - Interdisciplinary Centre for 3Rs in Animal Research, Faculty of Medicine, Justus-Liebig-University, Rudolf-Buchheim-Str. 6, 35392 Giessen, Germany; Peter.Jedlicka@informatik.med.uni-giessen.de
3 Institute of Clinical Neuroanatomy, Neuroscience Center, Goethe University, 60590 Frankfurt am Main, Germany
4 Frankfurt Institute for Advanced Studies, 60438 Frankfurt am Main, Germany
* Correspondence: wkilb@uni-mainz.de; Tel.: +49-211-3926-101

Received: 13 February 2019; Accepted: 18 March 2019; Published: 20 March 2019

Abstract: The effects of ionotropic γ-aminobutyric acid receptor (GABA-A, $GABA_A$) activation depends critically on the Cl^--gradient across neuronal membranes. Previous studies demonstrated that the intracellular Cl^--concentration ($[Cl^-]_i$) is not stable but shows a considerable amount of activity-dependent plasticity. To characterize how membrane properties and different molecules that are directly or indirectly involved in GABAergic synaptic transmission affect GABA-induced $[Cl^-]_i$ changes, we performed compartmental modeling in the NEURON environment. These simulations demonstrate that GABA-induced $[Cl^-]_i$ changes decrease at higher membrane resistance, revealing a sigmoidal dependency between both parameters. Increase in GABAergic conductivity enhances $[Cl^-]_i$ with a logarithmic dependency, while increasing the decay time of $GABA_A$ receptors leads to a nearly linear enhancement of the $[Cl^-]_i$ changes. Implementing physiological levels of HCO_3^--conductivity to $GABA_A$ receptors enhances the $[Cl^-]_i$ changes over a wide range of $[Cl^-]_i$, but this effect depends on the stability of the HCO_3^- gradient and the intracellular pH. Finally, these simulations show that pure diffusional Cl^--elimination from dendrites is slow and that a high activity of Cl^--transport is required to improve the spatiotemporal restriction of GABA-induced $[Cl^-]_i$ changes. In summary, these simulations revealed a complex interplay between several key factors that influence GABA-induced $[Cl]_i$ changes. The results suggest that some of these factors, including high resting $[Cl^-]_i$, high input resistance, slow decay time of $GABA_A$ receptors and dynamic HCO_3^- gradient, are specifically adapted in early postnatal neurons to facilitate limited activity-dependent $[Cl^-]_i$ decreases.

Keywords: development; hippocampus; CA3; Cl^--homeostasis; giant depolarizing potentials; ionic plasticity; computational neuroscience; Na^+-K^+-Cl^--Cotransporter, Isoform 1 (NKCC1); mouse

1. Introduction

GABA (γ-aminobutyric acid) is the main inhibitory neurotransmitter in the mature brain and acts via ionotropic $GABA_A$/$GABA_C$ receptors and via metabotropic $GABA_B$ receptors [1]. In the adult brain, GABA mediates its inhibitory effect by hyperpolarizing the membrane and by shunting excitatory inputs. $GABA_A$ receptors are ligand-gated anion-channels with a high permeability for Cl^-

ions and a considerable additional permeability for HCO_3^- ions [1]. In the mature brain the activity of a K^+-Cl^--Cotransporter (KCC, mainly in its isoform KCC2) establishes a low intracellular Cl^- concentration ($[Cl^-]_i$) [2,3], which accounts for a Cl^- influx and thus a membrane hyperpolarization upon activation of $GABA_A$ receptors [1]. Due to this Cl^--flux, activation of $GABA_A$ receptors can influence $[Cl^-]_i$ on a time scale of seconds to minutes [4–9], a process termed "ionic plasticity" [3,10,11]. The magnitude of activity-dependent $[Cl^-]_i$-transients depends on the Cl^- influx, dendritic volume and morphology, as well as on the capacity of Cl^- extrusion systems [12–17]. In addition, the membrane potential and the HCO_3^- permeability of $GABA_A$ receptors (P_{HCO_3}) contribute to the size of $[Cl^-]_i$ changes [6,18–20]. Therefore recent concepts of inhibition considered neuronal $[Cl^-]_i$ as a state- and compartment-dependent parameter of individual cells [14,20]. Detectable activity-dependent $[Cl^-]_i$ changes can occur in the adult nervous system under massive GABAergic stimulation [12,21]. However, already small alterations in $[Cl^-]_i$ or in the dynamics of the $[Cl^-]_i$ homeostasis critically influence information processing in neurons [20,22]. As the proper function in the adult nervous system relies on adequate inhibition [1,23,24], these activity-dependent $[Cl^-]_i$ changes play important roles in physiological and pathophysiological processes [10,11,17].

In the immature nervous system GABA typically induces depolarizing membrane responses [25–30]. These depolarizing GABAergic responses are caused by an elevated intracellular Cl^- concentration ($[Cl^-]_i$), which is maintained by a Cl^- accumulation via the isoform 1 of the Na^+-dependent K^+-Cl^--cotransporter (NKCC1) [3,29,31,32]. Recent studies suggest that at least in the postnatal neocortex, these depolarizing GABAergic responses mainly mediate inhibition [30,33], likely by increasing membrane shunting [1,34]. Several results indicate that depolarizing GABAergic neurotransmission is of specific relevance for immature spontaneous activity and for the maturation of the central nervous system [35–37]. Giant depolarizing potentials (GDPs) are a well-described network phenomenon in the immature hippocampus and the neocortex that represent spontaneous GABA-dependent activity [25,38,39]. In line with the high $[Cl^-]_i$ and the depolarizing responses, activation of $GABA_A$ receptors causes a decline in $[Cl^-]_i$ of immature neurons [29,40–42]. This attenuation of the $[Cl^-]$ gradient reduces possible excitatory effects of GABA [29,42,43] and may serve to limit GABAergic excitation and/or to stabilize recurrent network events [10,13,40]. A recent study demonstrated that GDPs, which are associated with a high amount of GABAergic activity [25,44], induce long-lasting $[Cl^-]_i$ transients and influence the steady-state $[Cl^-]_i$ of CA3 pyramidal neurons in hippocampal slices from early postnatal mice neurons [45], making it a suitable model for ionic plasticity in the immature brain.

However, while the existence of ionic plasticity is well accepted and several factors influencing activity-dependent $[Cl^-]_i$ transients have been described, the role of biophysical membrane characteristics, molecular properties of $GABA_A$-receptors or Cl^--transporters, and the stability of HCO_3^- homeostasis on ionic plasticity has not yet been systematically investigated. Here we used a detailed biophysical compartmental model in the NEURON environment to demonstrate how cellular and molecular properties such as input resistance, pH, HCO_3^--selectivity, kinetics of $GABA_A$ receptors, the kinetics of NKCC1 mediated Cl^- transmembrane transport, and the activity of carbonic anhydrases influence activity-dependent $[Cl^-]_i$ transients. While most modeling is performed in isolated dendritic compartments, here we also replicate the well-described GDP-induced $[Cl^-]_i$ transients of immature hippocampal CA3 neurons [45].

2. Results

In order to study the question how various membrane parameters and the properties of different molecules involved in GABAergic transmission influence activity-dependent $[Cl^-]_i$ transients, we first computed the GABA-induced $[Cl^-]_i$ changes in an isolated dendrite, which allows a better mechanistic understanding of the underlying processes. Subsequently we also used a model of a reconstructed CA3 pyramidal neuron [45] to compare the results of our computational models with the GDP-dependent $[Cl^-]_i$ transients recorded in immature hippocampal CA3 neurons [45]. For the latter

model, we implemented experimentally derived parameters of GABAergic synapses and GDP-activity provided by Lombardi et al. [45].

2.1. Influence of Membrane Conductance

First, we analyzed the influence of the membrane conductance on the $[Cl^-]_i$ changes induced by a single GABAergic input in an isolated dendrite. In this model, the experimentally determined conductance underlying single spontaneous GABAergic postsynaptic responses (g_{GABA}) was implemented in an isolated dendrite equipped with passive conductances (g_{pas}) varying between 10^{-6} S/cm^2 and 0.1 S/cm^2. These passive conductances correspond to input resistances (R_{Input}) between ca. 670 MΩ and 0.67 kΩ, respectively, when they were implemented in a reconstructed CA3 pyramidal neuron. The results of this experiment demonstrated that upon stimulation of a single GABAergic input (g_{GABA} = 0.789 nS, τ = 37 ms, P_{HCO_3} = 0, $[Cl^-]_i$ = 30 mM) not only the depolarization, but also the GABA-induced $[Cl^-]_i$ transient depended on the passive conductances. A detailed analysis revealed a strong, sigmoidal dependency between R_{Input} and peak $[Cl^-]_i$ changes (Figure 1a) or depolarization (Figure 1b) upon a single GABA stimulus. This effect of g_{pas} on the GABA-induced $[Cl^-]_i$ transients was caused by the fact that at lower g_{pas} the GABAergic currents induced a substantial depolarization, which attenuated the electromotive force on Cl^- ions (DF_{Cl}) during GABA stimulation (Figure 1c). At a low g_{pas} of 10^{-7} S/cm^2 (corresponding to a R_{input} of ca. 4 GΩ in the reconstructed neuron) the GABAergic depolarization reached E_{Cl} (Figure 1c, solid lines). Therefore, DF_{Cl} approximated 0 and no persistent Cl^- fluxes occurred. In contrast, at a g_{pas} of 0.018 S/cm^2 (corresponding to R_{input} of ca. 41 MΩ) E_m remained negative to E_{Cl}, thus enabling permanent Cl^- fluxes (Figure 1c, dashed lines).

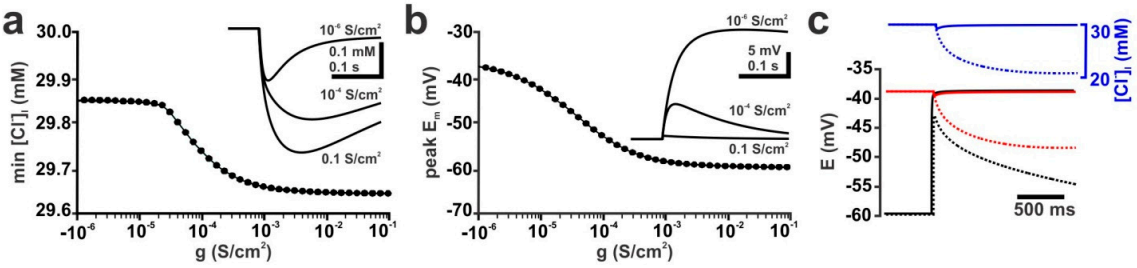

Figure 1. Passive membrane conductance (g_{pas}) influences GABA-induced $[Cl^-]_i$ transients. At low g_{pas} values, GABAergic currents induce strong depolarization, attenuating the driving force for Cl^- ions and thereby decreasing Cl^- fluxes. (**a**) The $[Cl^-]_i$ transients induced by a single GABAergic stimulation (g = 0.789 nS, τ = 37 ms, P_{HCO_3} = 0, $[Cl^-]_i$ = 30 mM) show a strong dependency on g_{pas}. Three typical traces are displayed as inset. (**b**) The GABA-induced membrane depolarization also shows a sigmoidal dependency on g_{pas}. (**c**) Effect of g_{pas} on E_m (black lines), E_{Cl} (red lines) and $[Cl^-]_i$ (blue lines) in an isolated dendrite using constant GABAergic currents (g_{GABA} = 0.1 µS). Note that at low g_{pas} values (0.1 nS/cm^2, solid lines) E_m approximates E_{Cl}, while at high g_{pas} (18 mS/cm^2, dashed lines) E_m stays below E_{Cl}. Accordingly $[Cl^-]_i$ shows only a small transient change at low g_{pas}, while a steady decline in $[Cl^-]_i$ occurs at high g_{pas}.

Next we simulated how g_{pas} influences $[Cl^-]_i$ in a reconstructed neuron (Figure 2a,b), which receives complex GABAergic inputs that typically occur during GDP activity [45] (Figure 2c,d). For these experiments we initially equipped the dendrite with 101 GABAergic synapses (g = 0.789 nS, τ = 37 ms; all values from Lombardi et al. [45]), set P_{HCO_3} to 0 and used an initial $[Cl^-]_i$ to 30 mM. Each of these 101 GABAergic synapses was randomly distributed within the dendrites of the reconstructed neuron. The time points for the stimulation of every synapse follows a normal distribution (µ = 600ms, σ = 900 ms). These values were derived from in-vitro experiments and resemble the distribution of GABAergic inputs during a GDP [45] (Figure 2c). In order to reduce the complexity of the analysis and to mimic the procedures of $[Cl^-]_i$ estimation used by Lombardi et al. [45] (which estimated $[Cl^-]_i$ changes from changes in E_{Rev} determined by focal GABA

application within the dendritic compartment) we use for all further analyses the average $[Cl^-]_i$ of all dendrites.

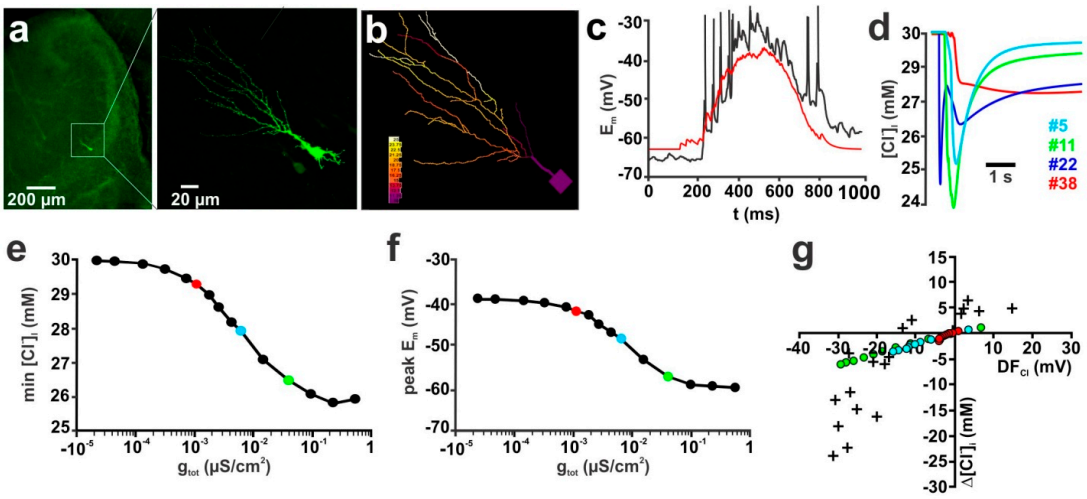

Figure 2. Passive membrane conductance (g_{pas}) influences GABA-induced $[Cl^-]_i$ transients in a reconstructed CA3 pyramidal neuron. Similar to the simulations in the isolated dendrite (Figure 1), GABAergic depolarization during a GDP approaches ECl at low g_{pas} values, thereby minimizing the driving force for Cl^- fluxes. (**a**) Immunofluorescence image of a biocytin labeled CA3 pyramidal neuron. (**b**) Reconstruction of this CA3 neuron as instrumented for NEURON simulation, with the colors representing the $[Cl^-]_i$ during an exemplary GDP. (**c**) Typical E_m trace of a GDP recorded in a real CA3 pyramidal neuron (black trace) and a simulated E_m trace of the reconstructed neuron upon stimulation with GDP-derived parameters (red trace). (**d**) Representative $[Cl^-]_i$ transients during a GDP displayed for 4 arbitrary dendrites. Note the asynchronous onset of individual $[Cl^-]_i$ transients and that $[Cl^-]_i$ transients are composed of synaptic Cl^- influx and diffusion from adjacent elements. (**e**) The average dendritic $[Cl^-]_i$ depends on the total conductance (g_{tot}) of the simulated cell. Please note that a cell that resembles the passive conductance of an immature hippocampal neurons (red symbol: R_{Input} = 901 MΩ) shows only a marginal $[Cl^-]_i$ decrease, while in cells equipped with a mature g_{pas} (cyan symbol: R_{Input} = 189 MΩ, green symbol: R_{Input} = 41 MΩ) larger GPD-induced $[Cl^-]_i$ transients occur. (**f**) Effect of g_{tot} on the peak depolarization during a GDP. Symbols are marked as indicated in (**e**). (**g**) Relationship between GABAergic driving force (DF_{Cl}) and GDP-induced $[Cl^-]_i$ transients. The crosses mark values determined experimentally in real CA3 pyramidal neurons. The colored cycles displays the $[Cl^-]_i$ changes computed for the three given R_{Input} values as indicated in (**e**). Note that for the immature R_{Input} only negligible GPD-induced $[Cl^-]_i$ changes are generated (a, b and c modified and used with permission from [45]).

Using this model, we investigated how different g_{pas} between 10^{-6} S/cm^2 and 0.1 S/cm^2 affect the GDP-induced $[Cl^-]_i$ transients. This simulation demonstrated that also in a complex dendritic compartment g_{pas} critically influenced the amount of $[Cl^-]_i$ changes (Figure 2e). Also, under these conditions the GABAergic depolarization during a GDP approached E_{Cl} at low g_{pas} (Figure 2f), which minimized DF_{Cl} and the remaining Cl^- fluxes. One particular result of this computational study was that the GDP-induced $[Cl^-]_i$ transient amounts to less than 1 mM in a reconstructed CA3 pyramidal neuron equipped with the passive membrane conductance determined experimentally in these neurons (red symbols in Figure 2e–g), which is lower than the experimentally determined $[Cl^-]_i$ changes of 10.3 ± 3.3 mM (n = 4) in a real CA3 pyramidal neuron at comparable conditions [45]. To further specify the influence of g_{pas} on the GDP-induced $[Cl^-]_i$ transients, we simulated the peak dendritic $[Cl^-]_i$ change for different initial $[Cl^-]_i$ at three different g_{pas}. For this purpose we used values of 0.049 mS/cm^2 (corresponding to a R_{Input} of 901 MΩ, typical for immature hippocampal neurons [45]), 0.28 mS/cm^2 (189 MΩ, adult neuron in whole-cell patch-clamp configuration [46]), and 1.8 mS/cm^2 (41 MΩ, adult neuron with sharp electrode [47]). These simulations demonstrated

that, if mature properties of g_{pas} were implemented in the simulated neuron, the GDP-induced $[Cl^-]_i$ changes were roughly comparable to the values observed in real CA3 pyramidal neurons (Figure 2g), while at g_{pas} typical for immature CA3 pyramidal neurons only marginal GDP-induced $[Cl^-]_i$ changes occurred.

In order to adapt the simulation of GDP-induced responses to the physiological properties of CA3 pyramidal neurons we incorporated an inward rectification in the background conductance (Supplementary Figure S1a,b). In addition, we had to increase the number of GABAergic synaptic inputs (n_{GABA}) to compensate the influence of massive space clamp problems on the experimental determination of this parameter (Supplementary Figure S1c–f). For all further simulations in the reconstructed neurons we used the inward rectifying background conductance and implemented 302, 395, and 523 GABAergic synapses for P_{HCO_3} values of 0.0, 0.18, and 0.44, respectively. However, even with the inward rectifying conductance and 302 synaptic inputs the GDP-induced $[Cl^-]_i$ changes were smaller than observed under in-vitro conditions (Supplementary Figure S1e).

2.2. Influence of GABA Receptor Conductivity and Kinetics

Next we analyzed the influence of the GABAergic conductance (g_{GABA}) on $[Cl^-]_i$ transients. Initial experiments in an isolated dendrite showed that initially the $[Cl^-]_i$ transient was localized underneath the synapse, and within 3 s a diffusional equilibration throughout the dendrite occurred (Supplementary Figure S2a,b). Therefore, we estimated the total amount of GABA-evoked $[Cl^-]_i$ changes by averaging the $[Cl^-]_i$ over all nodes of the dendrite 3 s after the GABAergic stimulus. To analyze the relation between total g_{GABA} and the $[Cl^-]_i$ changes, we first systematically increase g_{GABA} from 0.789 nS to 78.9 nS (Figure 3a). These simulations demonstrated that the GABA-evoked $[Cl^-]_i$ changes rose with increasing g_{GABA}, but did not depend linearly on g_{GABA} (Figure 3b, black line). This nonlinear effect was due to the larger membrane depolarization upon stronger GABAergic stimulation, which reduced DF_{Cl} under this condition (data not shown). In an additional set of simulations, we enhanced the level of GABAergic stimulation by increasing the number of GABAergic synapses (n_{GABA}) from 1 to 100, with g_{GABA} of 0.789 nS for each synapse. The synapses were for each n_{GABA} evenly distributed across the isolated dendrite. These simulations revealed that this distributed stimulation led to a reduced relative $[Cl^-]_i$ decrease at higher n_{GABA} (Figure 3b, red line), as compared to the previous simulation paradigm (Figure 3b, black line). This observation is most probably due to the fact that with distributed synapses E_m reaches more depolarized values close to E_{Cl} (-56.9 mV at 1×78.9 nS vs. -40.7 mV at 100×0.789 nS, data not shown).

To investigate whether a similar dependency between the amount of GABAergic inputs and $[Cl^-]_i$ could also be observed during a simulated GDP in a CA3 pyramidal neuron we increased g_{GABA} from 0.789 nS (Figure 3c, blue line) to 7.89 nS (red line) at each of the 302 synapses used to simulate a GDP. This 10× increase in g_{GABA} augmented the maximal GDP-induced $[Cl^-]_i$ decrease from 4.3 mM to 6.8 mM (Figure 3d). This surprisingly small effect was due to the fact that the increased g_{GABA} also reduced the average DF_{Cl} from -8.6 mV to -5 mV (Figure 3d). When a similar increase in the amount of GABAergic stimulation was implemented by a 10× increase in n_{GABA} (from 301 to 3010) a slightly larger maximal $[Cl^-]_i$ decrease by 7.1 mM was observed (Figure 3c,d, green line/symbols). This result indicates that the GDP-induced $[Cl^-]_i$ changes were close to saturation values when realistic values for n_{GABA}, g_{GABA} and R_{Input} were implemented in a simulated CA3 pyramidal neuron.

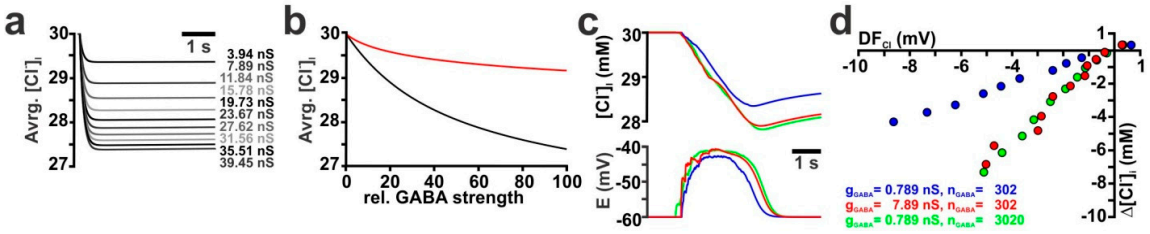

Figure 3. Influence of the GABAergic conductance (g_{GABA}) on GABA-induced $[Cl^-]_i$ transients. (**a**) Time course of average $[Cl^-]_i$ in an isolated dendrite upon single synaptic stimulation using g_{GABA} between 3.945 nS and 39.45 nS. (**b**) Average $[Cl^-]_i$ in an isolated dendrite stimulated at a single synapse with g_{GABA} between 0.789 nS (red trace) and 78.9 nS (black trace). Note the non-linear dependency between $[Cl^-]_i$ changes and g_{GABA}. In an additional set of simulations, the total GABAergic current was varied by increasing the number (n_{GABA}) of evenly distributed single synapses (with g_{GABA} = 0.789 nS) from 1 to 100 (red trace). Note that under these conditions, smaller $[Cl^-]_i$ changes occur. (c) GDP-induced average $[Cl^-]_i$ and E_m changes in a reconstructed CA3 pyramidal neuron under control conditions (τ = 37 ms, P_{HCO_3} = 0, g_{GABA} = 0.789 nS, n_{GABA} = 302, blue trace) and upon enhanced stimulation by either increasing the conductance (g_{GABA} = 7.89 nS, n_{GABA} = 302, red trace) or the number of synapses (g_{GABA} = 0.789 nS, n_{GABA} = 3020, green trace). (**d**) Dependency between DF_{Cl} and the GDP-induced $[Cl^-]_i$ transients obtained with different stimulation conditions.

In addition, we simulated how changes in the decay kinetics of $GABA_A$ receptor-mediated currents (τ_{GABA}) influence the $[Cl^-]_i$ transients (Supplementary Figure S2c,d). Systematic variation of τ_{GABA} between 10 ms and 1000 ms for a single synapse (g_{GABA} = 0.789 nS) in an isolated dendrite revealed that the average $[Cl^-]_i$ showed a nearly linear dependency on τ_{GABA} (Figure 4a, black line). If g_{GABA} was increased by a factor of 20 (g_{GABA} = 15.78 nS) the average $[Cl^-]_i$ concentration still showed a nearly linear dependency on τ_{GABA} (Figure 4a, red line). Since these responses suggested a strong influence of τ_{GABA} on the GABA-induced Cl^- fluxes, we also varied τ_{GABA} of all GABAergic synapses that were implemented on the reconstructed CA3 pyramidal neurons. These simulations revealed that an increase in τ_{GABA} indeed increased the GDP-induced $[Cl^-]_i$ changes (Figure 4b). The maximal GDP-induced decline in $[Cl^-]_i$ increases from 1.3 mM to 4.3 mM and 10.4 mM for τ_{GABA} of 3.7 ms, 37 ms and 370 ms, respectively (Figure 4c).

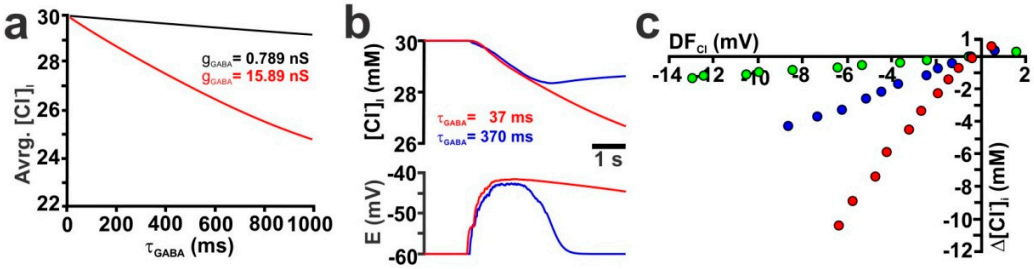

Figure 4. Influence of the decay time constant of GABA receptors (τ_{GABA}) on GABA-induced $[Cl^-]_i$ transients. (**a**) Relationship between average $[Cl^-]_i$ and τ_{GABA} at g_{GABA} of 0.789 nS (black trace) or 15.78 nS (red trace) upon a single synaptic stimulation (P_{HCO_3} = 0, $[Cl^-]_i$ = 30 mM) in an isolated dendrite. (**b**) GDP-induced average $[Cl^-]_i$ and E_m changes (n_{GABA} = 302, g_{GABA} = 0.789 nS, P_{HCO_3} = 0) using τ_{GABA} of 37 ms (red trace) and 370 ms (blue trace) in a reconstructed CA3 pyramidal neuron. (**c**) Relationship between DF_{Cl} and the GDP-induced $[Cl^-]_i$ transients obtained with different τ_{GABA} of 3.7 ms (green), 37 ms (blue) and 370 ms (red).

2.3. Contribution of the HCO_3^- Conductance of GABA Receptors

In all previous experiments, we simulated $GABA_A$ mediated responses under the simplified consideration that $GABA_A$ receptors are ligand-gated Cl^- channels. However, $GABA_A$ receptors are anion channels with a considerable HCO_3^- permeability [1]. The relative HCO_3^--permeability of

$GABA_A$ receptors (P_{HCO_3}) ranges between 0.18 (determined in spinal cord neurons [48]) and 0.44 (determined in adult hippocampal neurons [49]), although also higher values have been suggested [1]. Therefore, we next simulated how P_{HCO_3} affects GABAergic E_m and $[Cl^-]_i$ responses upon stimulation of a single synapse in an isolated dendrite. Addition of a HCO_3^- conductance to GABAergic currents induce a depolarizing shift in the peak depolarizations induced by GABAergic stimulation (Supplementary Figure S3a,b). Since this additional depolarization affected the DF_{Cl}, the GABAergic $[Cl^-]_i$ changes were also influenced by P_{HCO_3}. Under particular conditions, i.e. when E_m crossed E_{Cl} during synaptic responses, the GABAergic activation lead to biphasic $[Cl^-]_i$ changes (Figure 5a). For further analysis we plotted for such biphasic responses the maximal and minimal $[Cl^-]_i$ upon GABAergic stimulation (e.g. Figure 5b, blue lines). A systematic analysis of the effect of GABAergic inputs on the $[Cl^-]_i$ changes revealed that the $[Cl^-]_i$ changes were shifted towards more outward fluxes at higher P_{HCO_3} (Figure 5b), indicating that with increasing P_{HCO_3} a substantial $[Cl^-]_i$ increase is induced by GABAergic stimulation.

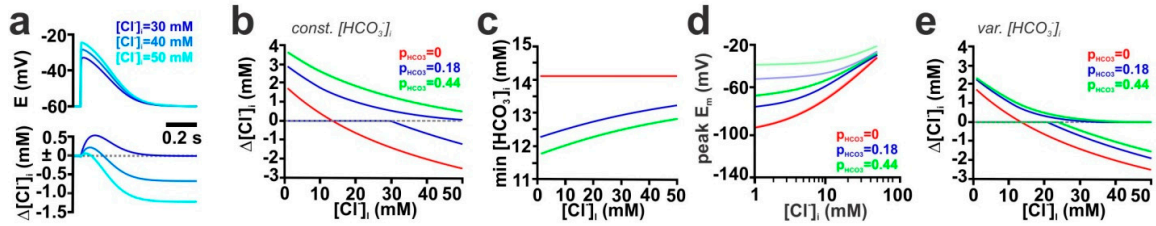

Figure 5. Influence of the relative HCO_3^- conductivity (P_{HCO_3}) on GABA-induced membrane depolarization and $[Cl^-]_i$ transients in an isolated dendrite. Activity-dependent decline in $[HCO_3^-]_i$ reduces GABAergic depolarization and affects $[Cl^-]_i$ changes. (**a**) Time course of E_m and $[Cl^-]_i$ changes ($\Delta[Cl^-]_i$) upon a single synaptic stimulation (g_{GABA} = 7.89 nS, τ = 37 ms, P_{HCO_3} = 0.18, $[HCO_3^-]_i$ = 14.1 mM) at initial $[Cl^-]_i$ of 30 mM (dark blue), 40 mM (middle) and 50 mM (light blue). Note that at intermediate $[Cl^-]_i$, a synaptic stimulus can induce biphasic $[Cl^-]_i$ responses. (**b**) Dependency between $\Delta[Cl^-]_i$ and $[Cl^-]_i$ upon a single synaptic stimulation (g_{GABA} = 7.89 nS, τ = 37 ms, $[HCO_3^-]_i$ = 14.1 mM) for different P_{HCO_3}. Note the biphasic responses for P_{HCO_3} of 0.18 (represented by the two blue lines) and that at higher P_{HCO_3} the $[Cl^-]_i$ fluxes are shifted towards influx even for high initial $[Cl^-]_i$. (**c**) Dependency between $[HCO_3^-]_i$ and $[Cl^-]_i$ upon a single synaptic stimulation using a model with dynamic $[HCO_3^-]_i$ (g_{GABA} = 7.89 nS, τ = 37 ms, initial $[Cl^-]_i$ = 30 mM, initial $[HCO_3^-]_i$ = 14.1 mM). (**d**) Dependency between peak depolarization and $[Cl^-]_i$ upon a single synaptic stimulation (conditions as in c) at different P_{HCO_3}. Note that the implementation of dynamic $[HCO_3^-]_i$ (plain lines) massively reduces peak depolarization as compared to conditions with static $[HCO_3^-]_i$ (shaded lines). (**e**) Dependency between $[Cl^-]_i$ changes and $[Cl^-]_i$ upon a single synaptic stimulation (conditions as in **c**). Dual lines with identical colors represent biphasic responses. Note the reduced $[Cl^-]_i$ changes with dynamic $[HCO_3^-]_i$ as compared to static $[HCO_3^-]_i$ conditions (shown in b) and that the $[Cl^-]_i$ at which Cl^- influx changes to Cl^- efflux was shifted to lower $[Cl^-]_i$.

However, these initial assumptions neglect the fact that the HCO_3^- fluxes will also affect $[HCO_3^-]_i$. Rapid regeneration of $[HCO_3^-]_i$ levels by carbonic anhydrases, which stabilize $[HCO_3^-]_i$, is absent in immature neurons [50]. Therefore, we first simulated the GABA-induced E_m and $[Cl^-]_i$ changes under the assumption that HCO_3^- will not be replenished (by implementing a HCO_3^- relaxation time constant ($\tau_{HCO_3^-}$) of 10 min) and is only redistributed by diffusion. These simulations revealed that the activation of $GABA_A$ receptors induced a rapid decline in $[HCO_3^-]_i$ (Supplementary Figure S3c). The $[HCO_3^-]_i$ decline depended on both P_{HCO_3} and $[Cl^-]_i$ and was maximal at low $[Cl^-]_i$ with values of 1.8 mM and 2.3 mM for P_{HCO_3} of 0.18 and 0.44, respectively (Figure 5c). In line with this $[HCO_3^-]_i$ decline, the GABAergic depolarization was drastically decreased (Figure 5d) under dynamic $[HCO_3^-]_i$ conditions. The attenuation of activity-dependent $[HCO_3^-]$ gradients also reduced the size of associated $[Cl^-]_i$ changes (Figure 5e) and at intermediate $[Cl^-]_i$ even reversed the effect (Supplementary Figure S3d).

As suggested from the results in isolated dendrites, the GDP-induced depolarization simulated in the reconstructed neuron was augmented if P_{HCO_3} was increased from 0.0 to 0.18 and 0.44 under the assumption of stable [HCO_3^-] gradients (Figure 6a,c, shaded symbols). And because under these conditions E_m could become positive to E_{Cl}, the Cl^- fluxes were enhanced and GDP-induced $[Cl^-]_i$ transients increased (Figure 6a,d, shaded symbols). Increasing P_{HCO_3} shifted the $[Cl^-]_i$ level at which GDP-induced $[Cl^-]_i$ transients change from influx to efflux, reflecting the impact of E_{HCO_3} on the DF_{CL}. The maximal influence of P_{HCO_3} on the $[Cl^-]_i$ changes was observed at low $[Cl^-]_i$ (Figure 6d, shaded symbols), because at these conditions, the depolarizing effect of HCO_3^- fluxes opposed the hyperpolarizing effects of E_{Cl}.

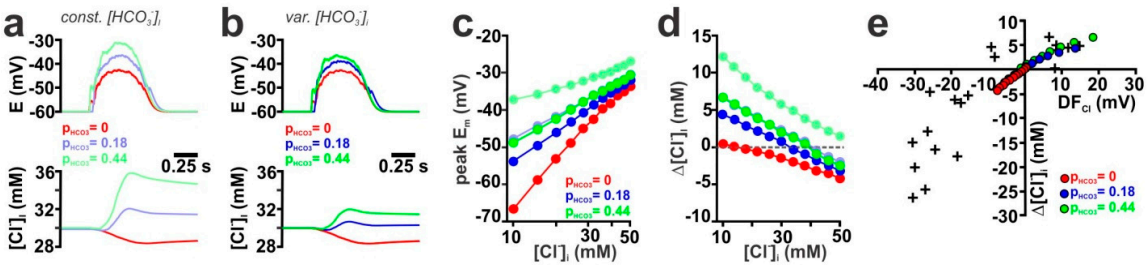

Figure 6. Influence of P_{HCO_3} on GABA-induced $[Cl^-]_i$ transients in a reconstructed CA3 pyramidal neuron. (**a**) Time course of E_m and average $[Cl^-]_i$ during a simulated GDP at different P_{HCO_3} (g_{GABA} = 0.789 nS, initial $[Cl^-]_i$ = 30 mM, $[HCO_3^-]_i$ = 14.1) using a model with a constant $[HCO_3^-]_i$. (**b**) E_m, average $[Cl^-]_i$ and $[HCO_3^-]_i$ during a simulated GDP at different P_{HCO_3} (g_{GABA} = 0.789 nS, initial $[Cl^-]_i$ = 30 mM,) using a model that implements dynamic $[HCO_3^-]_i$. Note that membrane depolarization and $[Cl^-]_i$ transients are diminished upon implementation of dynamic $[HCO_3^-]_i$. (**c**) Maximal E_m during a GDP at different initial $[Cl^-]_i$ and P_{HCO_3} using static (shaded lines) or dynamic $[HCO_3^-]_i$ (plain lines). (**d**) GDP-induced $[Cl^-]_i$ changes at different initial $[Cl^-]_i$ and P_{HCO_3} using static (shaded lines) or dynamic $[HCO_3^-]_i$ (plain lines). (**e**) Dependency between DF_{Cl} and the GDP-induced $[Cl^-]_i$ transients obtained with different P_{HCO_3} under dynamic $[HCO_3^-]_i$ conditions at P_{HCO_3} of 0 (red), 0.18 ms (blue) and 0.44 (green).

Implementation of a model that allowed dynamic $[HCO_3^-]_i$ changes (using a τ_{HCO_3} of 10 min) in the reconstructed CA3 pyramidal neuron showed that the GDP-induced GABAergic currents induced massive changes in $[HCO_3^-]_i$, depending on P_{HCO_3} (Supplementary Figure S3e). This GDP-induced $[HCO_3^-]_i$ decrease during a GDP diminished the membrane depolarization (Figure 6b,c, plain lines/symbols), which in turn caused a drastic reduction in the GDP-induced $[Cl^-]_i$ transients (Figure 6b,d, plain lines/symbols). In summary, addition of P_{HCO_3} to GABAergic currents augmented the DF_{Cl} and thus the GDP-induced $[Cl^-]_i$ transients (Figure 6e). Using these parameters, the simulated GDP-induced $[Cl^-]_i$ transients resembled the size of $[Cl^-]_i$ transients observed in real cells, however, only in the quadrant with positive DF_{Cl} values (Figure 6e).

2.4. The Stability of HCO_3^- Gradients Influences Activity-Dependent $[Cl^-]_i$ Transients

The previous results clearly demonstrate that $GABA_A$ receptor-mediated $[HCO_3^-]_i$ transients massively influence the E_m and $[Cl^-]_i$ changes under these conditions. However, the two conditions used in these experiments (stable $[HCO_3^-]_i$ or negligible $[HCO_3^-]_i$ regeneration at τ_{HCO_3} of 10 min) are obviously not physiological in immature neurons, which lack carbonic anhydrases, but in which spontaneous CO_2 hydration and/or transmembrane transport of HCO_3^- can occur [50]. Therefore, we next investigated how τ_{HCO_3} influences the stability of [HCO_3^-] gradients and GABA induced $[Cl^-]_i$ transients. For that we systematically changed the decay-time of $[HCO_3^-]_i$ relaxation (τ_{HCO_3}) implemented in the NEURON model (Supplementary Figure S4a,b). A systematic simulation in isolated dendrites revealed that $[Cl^-]_i$ changes remained rather constant at $\tau_{HCO_3} \geq 90$ ms (Figure 7a). The half-maximal $[Cl^-]_i$ changes occurred at a τ_{HCO_3} around 10 ms, which is substantially shorter than

the τ_{HCO_3} of ca. 70 ms for half-maximal $[HCO_3^-]_i$ changes (Supplementary Figure S4b). More than 85% of the maximal $[Cl^-]_i$ changes took place at τ_{HCO_3} below 100 ms (Figure 7a). However, it must also be considered that a decreased temporal stability of the $[HCO_3^-]$ gradient will also influence the lateral diffusion of HCO_3^-. Indeed, a systematic simulation of the spatial aspects of the activity-dependent $[HCO_3^-]_i$ transients revealed that the stability of HCO_3^- massively influenced the $[HCO_3^-]$ gradient along the isolated dendrite (Figure 7b), although the maximal $[HCO_3^-]_i$ change at the synaptic site was nearly saturated already at a $\tau_{HCO_3} \geq 90$ ms (Figure 7b). In accordance with the results obtained in isolated dendrites, also in the reconstructed CA3 pyramidal neuron τ_{HCO_3} had a large effect on the GDP-induced $[HCO_3^-]_i$ transients (Supplementary Figure S4c,d), but only a minor effect on the associated $[Cl^-]_i$ changes (Figure 7c). For $\tau_{HCO_3} \geq 90$ ms the GDP-induced $[Cl^-]_i$ changes were only marginally affected (Figure 7c, Supplementary Figure S4c) by changes in τ_{HCO_3}. At τ_{HCO_3} of 1 ms, the maximal GDP-induced $[Cl^-]_i$ decrease amounted to 5.2 mM, while it was 4.6 mM, 4.5 mM and 4.4 mM for τ_{HCO_3} values of 90 ms, 518 ms and 3 s, respectively. This small effect was also reflected by the minimal changes in the relation between DF_{Cl} and GDP-induced $[Cl^-]_i$ transients (Figure 7d).

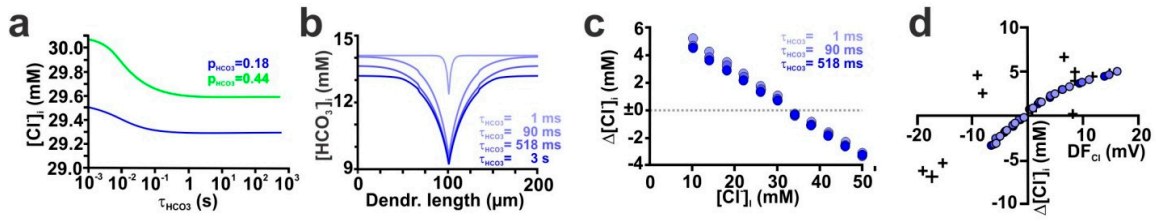

Figure 7. Influence of the stability of HCO_3^- gradients (via variations in τ_{HCO_3}) on GABA-induced membrane depolarization and $[Cl^-]_i$ transients. (**a**) Dependency between $[Cl^-]_i$ changes (determined 1 s after stimulus) and τ_{GABA} at P_{HCO_3} of 0.18 and 0.44 upon a single synaptic stimulation (g_{GABA} = 7.89 nS, τ = 37 ms, P_{HCO_3} = 0.18, initial $[Cl^-]_i$ = 30 mM) in an isolated dendrite. Note that at τ_{HCO_3} of ca. 1 s the maximal $[Cl^-]_i$ changes are reached. (**b**) Spatial profile of maximal $[HCO_3^-]_i$ changes upon the single synaptic stimulation (parameters as in a) at different τ_{HCO_3}. Note that τ_{HCO_3} influences the spatial profile of $[HCO_3^-]_i$, although the peak $[HCO_3^-]_i$ values are mainly comparable. (**c**) Dependency between maximal GDP-induced $[Cl^-]_i$ changes (g_{GABA} = 0.789 nS, τ = 37 ms, P_{HCO_3} = 0.18, n_{GABA} = 395, initial $[Cl^-]_i$ = 30 mM) and initial $[Cl^-]_i$ for different τ_{HCO_3} in the reconstructed CA3 pyramidal neuron. Note that the influence of τ_{HCO_3} on $[HCO_3^-]_i$ changes is largest at low $[Cl^-]_i$, but that overall τ_{HCO_3} has only a minimal impact on the $[Cl^-]_i$ changes. (**d**) Dependency between DF_{Cl} and the GDP-induced $[Cl^-]_i$ transients obtained with different τ_{HCO_3} (shadings as in **c**).

GABAergic [51] and glutamatergic [52,53] synaptic transmission is accompanied by substantial pH changes. These pH changes, however, indirectly affect GABAergic transmission, since they alter the $[HCO_3^-]_i$. To estimate, how such pH changes influence activity-dependent $[Cl^-]_i$ transients, we first simulated the effect of such pH shifts by constantly altering the pH value from 7.2 to 7.0 or 7.4 in an isolated dendrite. According to the Henderson-Hasselbalch equation, these pH shifts alter $[HCO_3^-]_i$ from 14.1 mM to 9 mM or 22.7 mM, respectively. Because this pH-dependent differences in $[HCO_3^-]_i$ affect DF_{GABA}, the membrane depolarization upon $GABA_A$ receptor activation was reduced at pH 7.0 and enhanced at a more alkaline pH of 7.4 (Figure 8a). In line with this altered GABAergic membrane depolarization, the DF_{Cl} during GABAergic stimulation was also affected, shifting the resulting Cl^- fluxes. This can be exemplified at intermediate $[Cl^-]_i$, where the biphasic Cl^- fluxes at a normal pH of 7.2, were transformed to Cl^- efflux at a pH of 7.0 and to a Cl^- influx at a pH of 7.4 (Figure 8a). A systematic analysis of Cl^- fluxes at different initial $[Cl^-]_i$ demonstrated that, in comparison to pH 7.2, the Cl^- influx at low initial $[Cl^-]_i$ was decreased at pH 7.0, while it was enhanced at pH 7.4 (Figure 8b). In contrast, the Cl^- efflux at high $[Cl^-]_i$ was enhanced at pH 7.0 and reduced at pH 7.4 (Figure 8d). In consequence, intracellular acidification shifted the $[Cl^-]_i$ range at which Cl^- efflux occurs to lower initial $[Cl^-]_i$, whereas intracellular alkalinization shifted this range to higher initial $[Cl^-]_i$ (Figure 8b).

Simulations in the reconstructed CA3 pyramidal neuron revealed that a lower pH of 7.0 led to smaller GDP-induced membrane depolarizations, as compared to the standard pH of 7.2 (Figure 8c, Supplementary Figure S4e, red line/symbols). This reduced depolarization resulted in a reduced GDP-associated Cl^- influx (4.6 mM vs. 7.6 mM) at low initial $[Cl^-]_i$ and in an increased Cl^- efflux (−6.1 mM vs. −4.3 mM) at high initial $[Cl^-]_i$ concentration (Figure 8d, red symbols). Conversely, at a higher pH of 7.4 the membrane responses during a GDP were more depolarized (Figure 8c, Supplementary Figure S4e green lines/symbols), which resulted in enhanced Cl^- influx of 11.2 mM at low initial $[Cl^-]_i$ and a decreased Cl^- efflux of −2.3 mM at low $[Cl^-]_i$ (Figure 8d, green symbols). In summary, these results demonstrate that the acidification associated with synaptic transmission reduced the activity-dependent $[Cl^-]_i$ transients at low $[Cl^-]_i$, while the activity-dependent Cl^- efflux at high $[Cl^-]_i$ was enhanced by such acidic shifts.

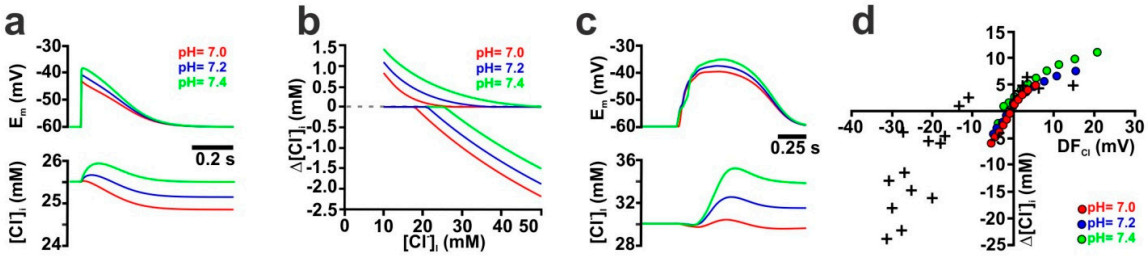

Figure 8. Influence of pH on GABA-induced membrane depolarization and $[Cl^-]_i$ transients. (**a**) Time course of E_m and $[Cl^-]_i$ upon a single synaptic stimulation (g_{GABA} = 7.89 nS, τ = 37 ms, P_{HCO_3} = 0.18, initial $[Cl^-]_i$ = 30 mM) in an isolated dendrite at different pH. Note the effect of pH on the depolarizations and that the biphasic $[Cl^-]_i$ at pH 7.2 was transformed into Cl^- efflux at pH 7.0 and to Cl^- influx at pH 7.4. (**b**) Dependency between GDP-induced $[Cl^-]_i$ changes and initial $[Cl^-]_i$ for different pH. For each pH the two lines represent maximal and minimal $[Cl^-]_i$ changes. Note that pH 7.0 shifts $[Cl^-]_i$ changes towards Cl^- efflux, whereas pH 7.4 shifts $[Cl^-]_i$ changes towards Cl^- influx. (**c**) Time course of GDP-induced depolarization and $[Cl^-]_i$ changes in the reconstructed CA3 pyramidal neuron (g_{GABA} = 0.789 nS, τ = 37 ms, P_{HCO_3} = 0.18, n_{GABA} = 395, initial $[Cl^-]_i$ = 30 mM) at different pH (color code as in a). Note that the GDP-induced $[Cl^-]_i$ changes are diminished at pH 7.0 and enhanced at pH 7.4. (**d**) Dependency between DF_{Cl} and the GDP-induced $[Cl^-]_i$ transients obtained at different pH. Note that at pH 7.0 the GDP-induced $[Cl^-]_i$ increase was diminished, while the $[Cl^-]_i$ decrease was slightly enhanced.

2.5. Influence of Transmembrane Cl^- Transport

Finally, we analyzed how the kinetics of the $[Cl^-]_i$ homeostasis influenced the temporal and spatial constrains of the activity-dependent $[Cl^-]_i$ changes. For that we systematically changed the decay-time of the $[Cl^-]_i$ relaxation (τ_{Cl}) implemented in the NEURON model. Initial simulations in isolated and soma-attached dendrites revealed that for τ_{Cl} of ≥ 10 s the decay of $[Cl^-]_i$ response was dominated by diffusional exchange with the soma (Supplementary Figure S4f–h). At a τ_{Cl} of 321 s 99.2% of Cl^- fluxes were depleted by diffusional exchange with the soma, while at faster τ_{Cl} a substantial smaller fraction of only 83.5 % (τ_{Cl} = 10 s), 33.2 % (τ_{Cl} = 1 s) and 2.4% (τ_{Cl} = 100 ms) of the Cl^- fluxes was eliminated by diffusion from the dendrite to the soma. Analysis of the spatial distribution of $[Cl^-]_i$ along the dendrite revealed that τ_{Cl} also affects the size of activity-dependent $[Cl^-]_i$ changes at distant dendritic sites (Supplementary Figure S4i–k). The dominance of diffusional elimination of Cl^- was also reflected by the observation that at slow $\tau_{Cl} \leq$ 10s the $[Cl^-]_i$ was substantial lower at the proximal than at the distal end of the dendrite (Supplementary Figure S4i–k).

To analyze the influence of τ_{Cl} on the spatial aspects of the $[Cl^-]_i$ transients we implemented two simultaneous GABAergic inputs that were located equidistant to the $[Cl^-]_i$ recording site at distances of 10 µm, 30 µm, 100 µm and 300 µm and systematically increased τ_{Cl} from 1 ms to 220 s (Figure 9a). These simulations revealed not only that the maximal $[Cl^-]_i$ depended on the distance between GABAergic stimulation sites and the node of $[Cl^-]_i$ determination, but also that τ_{Cl} critically

influenced the $[Cl^-]_i$ change at a given distance to the stimulation sites (Figure 9a). This dependency between spatial restrictions of activity-dependent $[Cl^-]_i$ changes and τ_{Cl} was quantified by the τ_{Cl} at which half-maximal $[Cl^-]_i$ changes occur ($\tau^{Cl}{}_{50}$). If the distance of the GABAergic synapses was 10 µm $\tau^{Cl}{}_{50}$ amounted to 12 ms, and this $\tau^{Cl}{}_{50}$ increased to 60.5 ms, 726 ms and 4.6 s at synaptic distances of 30 µm, 100 µm and 300 µm, respectively. To analyze the temporal aspects of $[Cl^-]_i$ summation we simulated five consecutive GABA stimulations at frequencies (f_{GABA}) of 0.3 Hz, 1 Hz, 3 Hz and 10 Hz and determine the $[Cl^-]_i$ at the stimulation site, while systematically varying τ_{Cl} (Figure 9b). These simulations revealed a sigmoidal dependency between τ_{Cl} and the temporal summation of $[Cl^-]_i$. A larger amount of $[Cl^-]_i$ summation and a lower $\tau^{Cl}{}_{50}$ was observed at higher frequencies. The $\tau^{Cl}{}_{50}$ amounted to 1.9 s for f_{GABA} of 0.1 Hz, 931 ms for f_{GABA} of 1 Hz, 268 ms for f_{GABA} of 3 Hz, and 53 ms for f_{GABA} of 10 Hz. In summary, these results demonstrated that τ_{Cl} values of less than 1 s are required to prevent substantial activity-dependent $[Cl^-]_i$ changes in the spatial and/or temporal domain at $f_{GABA} \geq 1$Hz and less than 100 µm distance between synaptic sites.

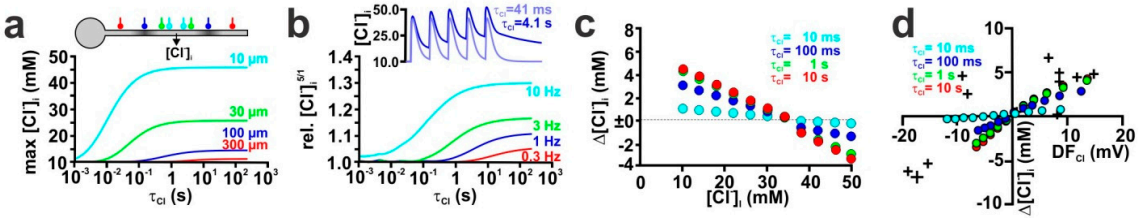

Figure 9. Influence of Cl^- diffusion and the kinetics of transmembrane Cl^- transport on GABA-induced $[Cl^-]_i$ transients. (**a**) Dependency between τ_{Cl} and $[Cl^-]_i$ determined in the middle between 2 simultaneously stimulated synapses (parameters as in a) located 10 µM, 30 µM, 100 µM and 100 µm from the node of $[Cl^-]_i$ recording. The inset represents a schematic illustration of the spatial arrangement. (**b**) Analysis of temporal summation of activity-dependent $[Cl^-]_i$ transients upon 5 consecutive GABA stimuli (parameters as in **a**) provided at frequencies of 0.3 Hz, 1 Hz, 3 Hz and 10 Hz in the dendrite + soma arrangement. The inset illustrates typical $[Cl^-]_i$ traces obtained at 3 Hz with τ_{Cl} of 41 ms and 4.1 s. The ratio in the $[Cl^-]_i$ between the first and fifth stimulus (rel. $[Cl^-]_i{}^{5/1}$) shows a sigmoidal dependency on τ_{Cl}. Note that with higher stimulus frequencies faster τ_{Cl} are required to prevent summation of $[Cl^-]_i$ transients. (**c**) Dependency between maximal GDP-induced $[Cl^-]_i$ changes (g_{GABA} = 0.789 nS, τ_{GABA} = 37 ms, P_{HCO_3} = 0.18, τ_{HCO_3} = 1 s, n_{GABA} = 395) and initial $[Cl^-]_i$ for different τ_{Cl} in the reconstructed CA3 neuron (**d**) Dependency between DF_{Cl} and the GDP-induced $[Cl^-]_i$ transients obtained with different $\tau_{Cl.}$

In accordance with these results in single dendrites, all previous simulations of GDP-induced $[Cl^-]_i$ transients in the reconstructed CA3 pyramidal cells revealed substantial $[Cl^-]_i$ changes, because in these simulations the experimentally determined τ_{Cl} of 174 s for NKCC1-mediated active Cl^- re-accumulation and of 321 s for passive Cl^- reduction were implemented and during a GDP stimulation a high frequency of GABAergic input was applied. In order to get more insights into how the capacity of $[Cl^-]_i$ regulation systems can influence activity-dependent $[Cl^-]_i$ transients within a realistic dendritic compartment, we finally simulated how different τ_{Cl} influenced the GDP-induced $[Cl^-]_i$ transients in the reconstructed CA3 neuron (Figure 9c,d). This simulation revealed that decreasing τ_{Cl} from the experimentally determined values >100 s to 10 s or 1 s had only a minimal impact of the GDP-induced $[Cl^-]_i$ transients (Figure 9c). The maximal GDP-induced $[Cl^-]_i$ change amounted to 4.41 mM at a τ_{Cl} of 10 s and to 4.21 mM at a τ_{Cl} of 1 s, but were reduced to 2.99 mM at a τ_{Cl} of 0.1 s and to 0.88 mM at a τ_{Cl} of 10 ms. These results demonstrate that fast and efficient $[Cl^-]_i$ homeostatic processes are required to limit GDP-induced $[Cl^-]_i$ transients. Accordingly, the $\Delta[Cl^-]_i$ vs. DF_{Cl} plot also revealed comparable GDP-induced $[Cl^-]_i$ changes at τ_{Cl} of 10 s and 1 s, and smaller $[Cl^-]_i$ changes at a τ_{Cl} of 100 ms (Figure 9d). Only a further reduction in τ_{Cl} to 10 ms substantially suppressed GDP-induced $[Cl^-]_i$ changes. In summary, these results indicate that τ_{Cl} influences the temporal and spatial properties of activity-dependent $[Cl^-]_i$ changes, but that τ_{Cl} values

that are substantially smaller than the experimentally determined values are required to suppress activity-dependent $[Cl^-]_i$ changes.

3. Discussion

In the present study we used a detailed biophysical compartmental modeling in the NEURON environment to systematically investigate how several cellular and molecular neuronal parameters influence the $GABA_A$ receptor-mediated $[Cl^-]_i$ changes. The main observations of this study can be summarized as follows: (i) A high R_{input} reduces activity-dependent $[Cl^-]_i$ transients, while at low R_{input} considerable activity-dependent $[Cl^-]_i$ transients can be observed. (ii) The activity-dependent $[Cl^-]_i$ transients show a logarithmic impact of g_{GABA}, while τ_{GABA} has in a wide g_{GABA} range a nearly linear influence on $[Cl^-]_i$. (iii) The P_{HCO_3} of $GABA_A$-receptors enhances activity-dependent $[Cl^-]_i$ transients, but with instable $[HCO_3^-]$ gradients this effect is largely diminished. (iv) Activity-dependent Cl^- fluxes where shifted toward efflux at acidic and towards influx at alkaline pH. (v) τ_{Cl} has a major impact on the spatiotemporal aspects of activity-dependent $[Cl^-]_i$ transients, but unrealistically fast τ_{Cl} values are required to prevent $[Cl^-]_i$ transients at physiologically-relevant activity levels.

By 1990, it was suggested by Qian and Sejnowski [54] that the Cl^- fluxes via activated $GABA_A$ receptors will dissipate the Cl^- gradient in small compartments and thus mediate potentially instable inhibitory responses. This theoretical assumption was proven by experimental studies, which demonstrated that massive GABAergic activation can shift hyperpolarizing responses toward depolarization [12,21] and induce $[Cl^-]_i$ transients [55]. In the past the physiological and pathophysiological consequences of such activity-dependent $[Cl^-]_i$ changes have been investigated and discussed [13,17,20,36,56] and the basic principles of activity-dependent $[Cl^-]_i$ changes and their implications for neuronal information processing have been modeled [7,15,16,22,57,58]. However, the complex interplay and contribution of passive membrane leak, $GABA_A$ conductance, Cl^- diffusion/transport and stability of $[HCO_3^-]$ gradients to these activity-dependent $[Cl^-]_i$ changes have not yet been systematically investigated.

Our simulations revealed a strong dependence between R_{Input} and the $GABA_A$ receptor induced $[Cl^-]_i$ transients. While at high R_{Input} GABA-induced $[Cl^-]_i$ changes were minimal, they increased in a nonlinear relation with decreasing R_{Input} (Figure 1c). This relation between R_{Input} and the $[Cl^-]_i$ changes is due to the fact that at high R_{Input} even small GABAergic currents bring E_m close to E_{Cl}, which minimizes DF_{Cl} and thus the Cl^- fluxes (Figure 1c). At low R_{Input} the passive membrane conductance stabilizes E_m and thus DF_{Cl}. In consequence, larger Cl^- fluxes can be expected. Accordingly, implementation of "adult like" membrane properties [47] in a reconstructed immature neuron massively enhanced activity-dependent $[Cl^-]_i$ changes (Figure 1c). In contrast, it seems obvious that immature neurons, with their high R_{Input} [59], are less susceptible to activity-dependent $[Cl^-]_i$ changes.

However, in this respect, it is important to consider that in immature neurons $[Cl^-]_i$ is high and GABAergic responses are depolarizing [30,60,61], therefore activity-dependent Cl^- fluxes are directed outward and are leading to $[Cl^-]_i$ decrease [42,44]. In addition, the HCO_3^--permeability of $GABA_A$ receptors also needs to be considered. The high R_{Input} in immature neurons causes E_m to approach E_{GABA}, which normally is positive to E_{Cl} due to the HCO_3^--permeability of $GABA_A$-receptors [1,4]. Therefore, stable Cl^- influx would be expected under this condition and $[Cl^-]_i$ should ultimately approach the value defined by E_{HCO_3}, which at steady-state HCO_3^- gradients ($[HCO_3^-]_i$ = 14.1 mM and $[HCO_3^-]_e$ = 26 mM) amounts to 72.4 mM. This estimation suggests that under certain conditions GABAergic activity can even increase $[Cl^-]_i$ from the already high $[Cl^-]_i$-levels in immature neurons (see Supplementary Figure S3d). But further properties of activity-dependent $[Cl^-]_i$ changes observed in our simulations protect immature neurons from excessive $[Cl^-]_i$ increases. In particular, we found that the influence of P_{HCO_3} is relatively small at high $[Cl^-]_i$ (Figure 6d), due to the fact that under this condition the contribution of E_{HCO_3} to E_{GABA} is small (as described by the

Goldman-Hodgkin-Katz-Equation [1]). In addition, in immature neurons the HCO_3^- gradient is instable because they lack carbonic anhydrases [50], which additionally attenuates the depolarizing effect of HCO_3^- on E_m and thus reduces DF_{Cl}.

Under the assumption of a stable HCO_3^- gradient, E_{GABA} is in a wide range positive to E_{Cl}, thereby permitting Cl^- influx during GABAergic stimulation, unless the thermodynamics equilibrium at 72.4 mM is reached. This is supported by the observation that no stable steady-state $[Cl^-]_i$ is reached with realistic $P_{HCO_3^-}$ values of 0.18 or 0.44 in our simulation (Supplementary Figure S3d, shaded lines). Experimental studies indeed demonstrated that massive GABAergic stimulation can shift E_{GABA} from hyperpolarizing towards depolarizing and even excitation [12,62–64]. On the other hand, if we implemented in our model that $[HCO_3^-]_i$ can be altered by $GABA_A$ receptors, the activity-dependent $[Cl^-]_i$ changes were massively reduced (Figure 5e). Our simulations also demonstrate that the switch from static $[HCO_3^-]$ to dynamic $[HCO_3^-]$ condition shifts the $[Cl^-]_i$ setpoint at which activity-dependent Cl^- influx was replaced by Cl^- efflux to considerably lower values (Figure 5e). This observation is due to the fact that the depolarizing HCO_3^- fluxes through the $GABA_A$ receptor are attenuated by the dissipating HCO_3^- gradient, which reduces E_{GABA} and thus DF_{Cl}. Similar conclusions were drawn from experiments in which a block of carbonic anhydrases with acetazolamide, which provides a pharmacological destabilization of $[HCO_3^-]$, also reduces E_{GABA} shifts ([18], but see [62]). We conclude from these observations that the lack of carbonic anhydrase VII in immature neurons [50,65] may serve to limit the activity-dependent $[Cl^-]_i$ changes in these neurons.

On the other hand, our simulations in a reconstructed CA3 pyramidal neuron revealed that although massive $[HCO_3^-]_i$ changes are induced under this condition, the total GDP-induced $[Cl^-]_i$ change was only marginally affected by variations in τ_{HCO_3} (Figure 7d). This lack of effect was most probably due to the fact that the activity-dependent $[HCO_3^-]_i$ change was already maximal at a τ_{HCO_3} of 90 ms at the synaptic site. This local saturated $[HCO_3^-]_i$ change at the subsynaptic site is the only determinant for the synaptic effects of the $[HCO_3^-]_i$. Our simulations also suggest that for an effective, physiologically relevant control of $[HCO_3^-]_i$ during GABAergic activity τ_{HCO_3} should be less than 70 ms (Supplementary Figure S4b). This fast relaxation time requires fast molecular processes that allow effective elimination of HCO_3^-. Indeed, carbonic anhydrases, the enzymes that mediate the degradation or regeneration of HCO_3^- into/from H_2O and CO_2, are among the fastest enzymes known. The k_{cat} of murine carbonic anhydrase VII for the hydration oh CO_2 is 4.5×10^5 s^{-1} at physiological pH [66]. From the assumption that the ca. 2mM $[HCO_3^-]_i$ change in the dendrite corresponds at a dendritic volume of 16 pL to ca. 0.3 fmol HCO_3^- ions, it can be estimated that about 4000 molecules of carbonic anhydrase VII are required to replenish the lost HCO_3^- within 100 ms. This estimation suggests that it is reasonable that sufficient carbonic anhydrase activity can be located in the dendritic compartment to reliably stabilize $[HCO_3^-]_i$. However, as the reaction mediated by carbonic anhydrases includes H^+ ions, the kinetics and thermodynamics of this process depends on the intracellular pH [67]. Thus dendritic H^+-buffering and handling indirectly also affects activity-dependent $[Cl^-]_i$ changes [15]. The acidification associated with neuronal activity [52,53] will slow down the kinetics of carbonic anhydrases [66]. However, this effect is negligible in comparison to the effect of the intracellular pH on $[HCO_3^-]_i$. The intracellular pH is an essential parameter that determines $[HCO_3^-]_i$ [67]. Thus the intracellular acidification observed upon activation of GABAergic and glutamatergic synapses [51–53] will alter $[HCO_3^-]_i$ and subsequently influence GABAergic transmission. Our simulation revealed that an intracellular acidification will reduce the activity-dependent $[Cl^-]_i$ changes at low $[Cl^-]_i$. This result, which is in accordance with a previous simulation [15], indicate that in adult neurons a parallel acidification will limit Cl^- influx and thus stabilize inhibitory transmission In contrast, at a high $[Cl^-]_i$ typical for immature neuron the intracellular acidification enhanced the activity-dependent Cl^- efflux and may contribute to the loss of depolarizing drive and putative excitatory effects after strong GABAergic stimulation.

Another factor that has a stringent effect on activity-dependent $[Cl^-]_i$ changes in our simulations is τ_{GABA}. This confirmed and extended previous computational analyses (c.f. Figure 4d in [7]). It has been

found that in general the decay kinetics of GABAergic transmission get faster during development [68]. Therefore the slow decay kinetics of GABAergic transmission in immature neurons [68,69] may be a factor that enables activity-dependent $[Cl^-]_i$ transients, while the faster GABAergic postsynaptic currents in mature neurons not only improve the temporal precision of GABAergic transmission [68], but also the stability of inhibition. While a stable inhibition is a prerequisite for the proper function of mature neuronal networks, dynamic changes in $[Cl^-]_i$ can be mandatory for physiological relevant functional features of the immature central nervous system. It has been suggested that activity-dependent changes in $[Cl^-]_i$, and the resulting switch from GABAergic inhibition to excitation, can underlie oscillatory activity [13]. In addition, in the immature nervous system the resting $[Cl^-]_i$ is decreased by GABAergic activity, which will result in a diminished excitatory drive and/or a dominance of shunting inhibition and may thus serve to limit a possible excitatory effect of GABA [40]. Therefore, for immature neurons an unstable $[Cl^-]_i$ homeostasis may be functionally relevant, as it allows activity-dependent scaling of $[Cl^-]_i$-dependent synaptic transmission [42,43].

In consequence, the molecular configuration of immature neurons (high $[Cl^-]_i$, long τ_{GABA} and missing CA-VII) will generate conditions that allow limited activity-dependent $[Cl^-]_i$ decreases. This, in addition to the aforementioned effect of the high input resistance, may be an explanation why the $[Cl^-]_i$ homeostasis of immature neurons is maintained by a relatively ineffective transmembrane Cl^- transport [29]. In contrast, in mature neurons the situation is different. In the adult brain, the low $[Cl^-]_i$ is needed to maintain hyperpolarizing inhibition [1] and an activity-dependent $[Cl^-]_i$ increase will attenuate membrane hyperpolarization. While it is obvious that massive changes in $[Cl^-]_i$ will impair GABAergic inhibition and can lead to hyperexcitability [18], recent modeling experiments demonstrate that even minimal changes in the capacity of Cl^--extrusion can have strong effects on information processing and storage in neurons [22]. Although the low R_{Input} and the fast τ_{GABA} counteracts activity-dependent $[Cl^-]_i$ increase in adult neurons, their low $[Cl^-]_i$ and their effective carbonic anhydrases can lead to substantial $[Cl^-]_i$ changes in their dendrite. The adverse effect of such local activity-dependent $[Cl^-]_i$ increases is enhanced by the more elaborated dendritic compartment in mature neurons, which limits diffusional elimination of Cl^--ions [13].

Our simulations reveal that the connection of an isolated dendrite to the soma drastically reduces the equilibrium $[Cl^-]_i$ after synaptic stimulation (Supplementary Figure S4f–k), demonstrating the important role of diffusional Cl^- elimination under this condition. The large volume to surface ratio (and thus volume to conductance ratio) of the soma enables this compartment to serve as Cl^- sink in these in-silico experiments. Also in-vitro it has been demonstrated that activation of dendritic $GABA_A$ receptors induced massive shifts in E_{GABA}, whereas only minimal changes were observed upon perisomatic stimulation [10,12,26]. The dominance of perisomatic GABAergic terminals [70] may be related to the requirement of stable $[Cl^-]$ gradients to maintain stable inhibition over a wide range of activity levels. However, the diffusion of $[Cl^-]_i$ through dendrite is a relatively slow and inefficient process, due to the small diameter in distal dendrites [7,55]. Addition of spines to dendrites drastically slow down diffusion along dendrites [16], suggesting that the complexity of the dendritic compartment (i.e. the number of arborizations that enhance tortuosity in the dendritic compartment) hinders Cl^--elimination by diffusion to the soma. Therefore, active elimination of Cl^- from the cytoplasm is required to prevent or minimize activity-dependent $[Cl^-]_i$ changes in the elaborated dendritic compartment of adult neurons.

The elementary role of transmembrane Cl^- transporters for neuronal $[Cl^-]_i$ homeostasis has been shown by a variety of studies [2,29,32,58,71]. Modeling studies revealed that slightly altered rates of transmembrane Cl^--transport, which does only marginally affect resting $[Cl^-]_i$ levels, have a strong effect on the spatiotemporal distribution of activity-dependent $[Cl^-]_i$-transients in dendrites [15]. Therefore it is not surprising that the simulation of an enhanced capacity of transmembrane Cl^- transport by increasing τ_{Cl} attenuates activity-dependent $[Cl^-]_i$ transients. However, to minimize these $[Cl^-]_i$ transients a rather low τ_{Cl} of < 100 ms is required. These low τ_{Cl} values are several orders of magnitude below the experimentally determined kinetics of the NKCC1-mediated Cl^--accumulation

(τ_{Cl} = 158 s) in immature neurons [29]. Because of this slow kinetic of transmembrane transport of Cl^- in immature neurons, we also consider that a Cl^-/HCO_3^- exchange mediated by the anion exchanger in immature neurons [72] has only a marginal effect on both activity-dependent $[Cl^-]_i$ and $[HCO_3^-]_i$ transients in these neurons. In the mature situation (low $[Cl^-]_i$ and effective transmembrane $[Cl^-]_i$ transport), modeling studies suggest that an interference between $[Cl^-]_i$ and $[HCO_3^-]_i$ by this mechanism can reduce the activity-dependent $[Cl^-]_i$ changes [15].

While it is generally assumed that the neuron-specific Cl^--extruder KCC2 mediates more efficient Cl^- transport than NKCC1, only few experimental studies addressed the kinetics of KCC2-dependent Cl^--extrusion. Experiments in brain stem neurons demonstrated that KCC2 mediated Cl^--extrusion after $[Cl^-]_i$ increase by ca. 10 mM requires several minutes [73]. In contrast, in-vivo experiments revealed that the activity-dependent $[Cl^-]_i$ increase after an epileptic seizure recovered within less than 30 s [9] and in hippocampal slices GABA-induced $[Cl^-]_i$ transients recovered back to low steady-stale levels with a time constant of 3.3 s [12]. However, it is not clear how diffusional processes and/or the kinetics of the used Cl^- sensor contribute to these kinetic properties. Simulations suggest that with realistic KCC2 levels τ_{Cl} in the distal dendrites ($\geq$ 200 µm from the soma) is between 100 ms and 200 ms [15], and thus probably lower than estimated from experimental data. Even this time constant is higher than the τ_{Cl} required in our simulations to prevent local activity-dependent $[Cl^-]_i$ changes, suggesting that considerable $[Cl^-]_i$ changes can occur at GABAergic synaptic sites. While our and other simulations [15] suggest these transients may be restricted to local dendritic domains, it must be emphasized that subtle changes in the efficacy of KCC2 mediated Cl^--transport can already enhance the excitability in single neurons because activity-dependent $[Cl^-]_i$ transients may superimpose these effects [22]. In consequence, impairments of KCC2 mediated Cl^- transport can led to a breakdown of sufficient inhibition in neuronal networks and contribute to hyperexcitability [15,17,20,56,74]. In this respect it is also relevant to consider that the activity of both NKCC1 and KCC2 are regulated by a variety of processes [75–78]. This indicates that the spatiotemporal $[Cl^-]_i$ dynamics in the dendritic compartment may be adapted to the functional states.

The limitation of our model to fully describe GDP-induced $[Cl^-]_i$ transients in CA3 pyramidal neurons is obvious from the fact, that we massively underestimate the $[Cl^-]_i$ decrease observed in real CA3 pyramidal neurons at high $[Cl^-]_i$ (e.g. Figure 6e). Therefore, additional factors must be proposed, which enhance the $GABA_A$-receptor-mediated Cl^- efflux. Possible mechanisms that improve Cl^- efflux are e.g. an inhomogeneous distribution of voltage-activated K^+ channels in the dendritic compartment, an underestimation of n_{GABA} in our in-vitro experiments due to voltage-clamp errors in the elaborated dendrite [79], or the effect of glutamatergic transmission during a GDP [20,80]. In addition, we also found that τ_{GABA} has a major impact on the GDP-induced $[Cl^-]_i$ transients, and it might well be that the decay kinetics of spontaneous GABAergic PSCs of 37 ms [45] reflect the kinetic properties of a subpopulation of GABAergic inputs, that is less involved in the generation of GDPs. Finally, in our simulations the dendrite was implemented as a hollow tube with a diameter determined from the histological reconstruction. Under realistic assumptions the neuron is, however, filled with cytoplasm that contains large proteins, particles of different sizes and vesicles and tubes of intracellular organelles. Thus the free, "unexcluded" volume in the cytoplasm is restricted to an estimated fraction of ca. 60%, a principle termed cytoplasmic crowding [81]. This restricted free cytoplasmic water volume will increase the size of $[Cl^-]_i$ transients upon identical Cl^- fluxes.

4. Materials and Methods

Compartmental Modeling

The biophysically realistic compartmental modelling was performed using the NEURON environment (neuron.yale.edu). The source code of models and stimulation files used in the present paper can be found in ModelDB [82] at http://modeldb.yale.edu/253369 (access date 14 March 2019) and was included in the supplementary material of this publication. For compartmental modelling we used either

a simple ball and stick model (soma with d = 20 µm, linear dendrite with l = 200 µm and 103 nodes) or a reconstructed CA3 pyramidal cell (from Lombardi et al. [45]). Except where noted the dendrite was detached from the soma to analyse dendritic $[Cl^-]_i$ transients. The reconstructed neuron resembled the somatodendritic morphology of a typical immature CA3 pyramidal neuron (see Figure 2a,b). For this purpose images of a biocytin-filled neuron [83,84] were taken with 60× oil-immersion objectives and the somatodendritic morphology was reconstructed using Fiji (www.fiji.sc). It contained a soma (d = 15 µm), a dendritic trunk (d = 2 µm, l = 32 µm, 9 segments) and 56 dendrites (d = 0.36 µm, 9 segments each). In all of these compartments a specific axial resistance (R_a) of 34.5 Ωcm and a specific membrane capacitance (C_m) of 1 µF cm^{-2}; were implemented. The specific membrane conductance (g_{pas}) varied (see Figures 1a and 2e) and in the majority of the experiments was modeled by a voltage dependent process given by a Boltzmann-like equation:

$$g_{pas} = g_{min} + \frac{g_{max}}{\left(1 + \exp\left(\frac{(E_m - E_{50})}{s}\right)\right)} \quad (1)$$

with g_{max} = 0.002800 S/cm^2 (experimentally determined g_{Input} at depolarized potentials, see Supplementary Figure S1a), gmin = 0.000660 S/cm^2 (experimentally determined minimal g_{Input} at hyperpolarized potentials, see Figure 3a), e50 = −31 mV (half-maximal voltage), s = −6 (slope of the voltage-dependency). The reversal potential of this voltage-depended g_{pas} was set to −60 mV.

$GABA_A$ synapses were simulated as a postsynaptic parallel Cl^- and HCO_3^- conductance with exponential rise and exponential decay [7]:

$$I_{GABA} = I_{Cl} + I_{HCO_3} = 1/(1+P)\ g_{GABA}\ (V\text{-}E_{Cl}) + P/(1+P)\ g_{GABA}\ (V\text{-}E_{HCO_3}) \quad (2)$$

where P is a fractional ionic conductance that was used to split the $GABA_A$ conductance (g_{GABA}) into Cl^- and HCO_3^- conductance. E_{Cl} and E_{HCO_3} were calculated from Nernst equation. The $GABA_A$ conductance was modeled using a two-term exponential function, using separate values of rise time (0.5 ms) and decay time (variable, mostly 37 ms) [45]. Parameters used in our simulations were as follows: $[Cl^-]_o$ = 133.5 mM, $[HCO_3^-]_i$ = 14.1 mM, $[HCO_3^-]_o$ = 24 mM, temperature = 31 °C, P = 0.44 [49]. For the ball and stick model a single $GABA_A$ synapse was placed in the middle of the dendrite, except where noted. For the simulation of a GDP in the reconstructed CA3 neuron 101–3020 GABAergic synapses were randomly distributed within the dendrites of the reconstructed neuron. GABA inputs were activated stochastically using a normal distribution (µ = 600ms, σ = 900 ms) that emulates the distribution of GABAergic PSCs during a GDP observed in immature hippocampal CA3 pyramidal neurons [45]. The properties of these synapses were always given in the results part and/or the corresponding figure legends.

From the quotient between the charge transfer of a GDP and of spontaneous GABAergic postsynaptic currents at a holding potential (V_{Hold}) of 0 mV it was estimated that 101 GABAergic inputs underlie a GDP [45]. To compensate for the space-clamp problems during a GDP, that were not considered by Lombardi et al. [45], we simulated the charge transfer during a GDP under their experimental conditions ($[Cl^-]_i$ = 10 mM, V_{Hold} = 0 mV) and determined that 302, 395, and 523 (for P_{HCO_3} values of 0.0, 0.18, and 0.44, respectively) GABAergic synapses are required to generate the observed GDP-induced charge transfer (Supplementary Figure S1c–f). For these experiments we implement the single-electrode voltage clamp procedure provided by NEURON, using an access resistance of 5 MΩ. The charge transfer was calculated from the integral of the holding currents (I_{Hold}) during the GDP.

For the modeling of the $GABA_A$ receptor-induced $[Cl^-]_i$ and $[HCO_3^-]_i$ changes, we calculated ion diffusion and uptake by standard compartmental diffusion modeling [16,85–87]. To simulate intracellular Cl^- and HCO_3^- dynamics, we adapted our previously published model [7]. Longitudinal Cl^- and HCO_3^- diffusion along dendrites was modeled as the exchange of anions between adjacent compartments. For radial diffusion, the volume was discretized into a series of 4 concentric shells around a cylindrical core [85] and Cl^- or HCO_3^- was allowed to flow between adjacent shells [88].

The free diffusion coefficient of Cl^- inside neurons was set to 2 $\mu m^2/ms$ [55,89]. Since the cytoplasmatic diffusion constant for HCO_3^- is, to our knowledge, unknown, we also used a value of 2 $\mu m^2/ms$. To simulate transmembrane transport of Cl^- and HCO_3^-, we implemented an exponential relaxation process for $[Cl^-]_i$ and $[HCO_3^-]_i$ to resting levels $[Cl^-]_i^{rest}$ or $[HCO_3^-]_i^{rest}$ with a time constant τ_{Ion}.

$$\frac{d[Ion^-]_i}{dt} = \frac{[Ion^-]_i^{rest} - e[Ion^-]_i}{\tau_{Ion}} \quad (3)$$

Cl^- transport was in most experiments (if not otherwise noted) modeled as bimodal process, for $[Cl^-]_i < [Cl^-]_i^{rest}$ τ_{Ion} was set to 174 s to emulate an NKCC1-like Cl^- transport mechanism. For $[Cl^-]_i > [Cl^-]_i^{rest}$ τ_{Ion} was set to 321 s to emulate passive Cl^- efflux (both values obtained from unpublished experiments on immature rat CA3 hippocampal neurons).

The impact of GABAergic Cl^- currents on $[Cl^-]_i$ and $[HCO_3^-]_i$ was calculated as:

$$\frac{d[Ion^-]_i}{dt} = \frac{1}{F}\frac{I_{Ion}}{volume} \quad (4)$$

To simulate the GABAergic activity during a GDP, a unitary peak conductance of 0.789 nS and a decay of 37 ms were applied to each GABAergic synapse. These values resulted in a unitary currents of pA, which was in accordance with the mean amplitude of spontaneous GABAergic postsynaptic currents in CA3 paramidal neurons [45].

For the isolated neurons the $[Cl^-]_i$ and $[HCO_3^-]_i$ concentration was averaged over all segments of the dendrite, except where noted. For the simulated neurons we analyzed mean $[Cl^-]_i$ and $[HCO_3^-]_i$ of all dendrites:

$$[Cl^-]_i = \frac{1}{n_{dend}} \times \sum_{j=1}^{n_{dend}} [Cl^-]_i^{Dend(j)\ @\ 0.5\ of\ total\ length} \quad (5)$$

This procedure mimics the experimental procedure of Lombardi et al [45], who determined E_{GABA} by focal application in the dendritic compartment.

For the calculation of $\Delta[Cl^-]_i$ the maximal deviation of $[Cl^-]_i$ upon a GABAergic stimulus ($[Cl^-]_i^S$) was subtracted from the resting $[Cl^-]_i$ before the stimulus ($[Cl^-]_i^R$). For biphasic responses both minimal and maximal $[Cl^-]_i^R$ were determined and $\Delta[Cl^-]_i$ was calculated as:

$$\Delta[Cl^-]_i = [Cl^-]_i^{S,\,min} - [Cl^-]_i^R \quad \text{if } abs\left([Cl^-]_i^{S,\,min}\right) > abs\left([Cl^-]_i^{S,\,max}\right) \quad (6)$$

$$\Delta[Cl^-]_i = [Cl^-]_i^{S,\,max} - [Cl^-]_i^R \quad \text{if } abs\left([Cl^-]_i^{S,\,min}\right) \leq abs\left([Cl^-]_i^{S,\,max}\right) \quad (7)$$

The driving-force of Cl^- (DF_{Cl}) was calculated from the difference between the average E_m during a GDP and E_{Cl} ($DF_{Cl} = E_m - E_{Cl}$). To calculate the ratio between transmembrane $[Cl^-]_i$ transport and diffusional $[Cl^-]_i$ depletion into the soma, we normalized the diffusional exchange between the last somatic node and the soma (as calculated from Fick's law) to conditions were transmembrane $[Cl^-]_i$ loss was absent ($\tau_{Cl} = 10^9$ ms) and diffusional dendrite to soma transport was allowed to equilibrate for 2 min.

All electrophysiological data were taken from our previous publication [45]. However, for a comparison of these results with the simulations, we had to take different P_{HCO_3} into account. Therefore the GDP-induced $[Cl^-]_i$ changes were recalculated using P_{HCO_3} values of 0.0, 0.18 (determined in spinal cord neurons [48]) and 0.44 (determined in adult hippocampal neurons [49]). The $[Cl^-]_i$ was calculated from E_{GABA} with the Goldman-Hodgkin-Katz equation:

$$E_{GGABA} = \frac{RT}{ZF} \times \ln\left(\frac{P_{Cl}[Cl^-]_e + P_{HCO_3}[HCO_3^-]_e}{P_{Cl}[Cl^-]_i + P_{HCO_3}[HCO_3^-]_i}\right) \quad (8)$$

For the calculation of $[Cl^-]_i$ from E_{GABA} we used a $[Cl^-]_e$ of 133.5 mM, an extracellular HCO_3^- concentration ($[HCO_3^-]_e$) of 24 mM and assumed a constant $[HCO_3^-]_i$ of 14.1 mM (calculated from an intracellular pH of 7.2 [90], a CO_2 pressure (pCO_2) of 38 mmHg, a Henry coefficient (α) of 0.0318 mM/mmHg and a pKs of 6.128 [91] with the Henderson-Hasselbalch equation), if not otherwise mentioned.

$$[HCO_3^-]_i = 10^{(pH-pKs+\log(\alpha \times pCO_2))} \quad (9)$$

R_{Input} was calculated from the E_m response upon a simulated current injection (I_{Inj}) according to Ohms law:

$$R_{Input} = \frac{E_m}{I_{Inj}} \quad (10)$$

Supplementary Materials: Supplementary materials can be found at http://www.mdpi.com/1422-0067/20/6/1416/s1.

Author Contributions: Conceptualization, P.J. and W.K.; Investigation, A.L. and W.K.; Coding, A.L., P.J. and W.K.; Writing—original draft, A.L., P.J., H.J.L. and W.K.; Writing—review and editing, P.J., H.J.L. and W.K.

Funding: This research was funded by grants of the Deutsche Forschungsgemeinschaft to WK (KI-835/3) and to HJL (CRC 1080) and by grants of the University Medical Center Giessen and Marburg (UKGM) to P.J.

Acknowledgments: The authors thank Beate Krumm for her excellent technical support. W.K. thanks Kristina and Benjamin for their patience.

Conflicts of Interest: The authors declare no conflict of interest.

Abbreviations

DF_{Cl}	Electromotive driving force on Cl^- ions
E_{Cl}	Equilibrium potential for Cl^-
E_{GABA}	Reversal potential of GABAergic currents
E_{HCO_3}	Equilibrium potential for HCO_3^-
GABA	γ-Amino butyric acid
GDP	Giant depolarizing potential
g_{GABA}	Conductance of GABAergic synapse
g_{pas}	Passive membrane conductance
KCC	K^+-Cl^--Cotransporter
NKCC1	Na^+-K^+-Cl^--Cotransporter, Isoform 1
n_{GABA}	Number of GABAergic synapses
P_{HCO_3}	Relative HCO_3^- permeability of $GABA_A$ receptors
V_{Hold}	Holding potential
τ_{Cl}	Time constant of $[Cl^-]$ relaxation
τ_{GABA}	Decay time constant of $GABA_A$ receptors
τ_{HCO_3}	Time constant of $[HCO_3^-]$ relaxation

References

1. Farrant, M.; Kaila, K. The cellular, molecular and ionic basis of GABA(A) receptor signaling. *Prog. Brain Res.* **2007**, *160*, 59–87. [PubMed]
2. Rivera, C.; Voipio, J.; Payne, J.A.; Ruusuvuori, E.; Lahtinen, H.; Lamsa, K.; Pirvola, U.; Saarma, M.; Kaila, K. The K^+/Cl^- co-transporter KCC2 renders GABA hyperpolarizing during neuronal maturation. *Nature* **1999**, *397*, 251–255. [CrossRef] [PubMed]
3. Blaesse, P.; Airaksinen, M.S.; Rivera, C.; Kaila, K. Cation-chloride cotransporters and neuronal function. *Neuron* **2009**, *61*, 820–838. [CrossRef]
4. Kaila, K.; Pasternack, M.; Saarikoski, J.; Voipio, J. Influence of GABA-gated bicarbonate conductance on potential, current and intracellular chloride in crayfish muscle fibres. *J. Physiol.* **1989**, *416*, 161–181. [CrossRef] [PubMed]

5. Bracci, E.; Vreugdenhil, M.; Hack, S.P.; Jefferys, J.G.R. Dynamic modulation of excitation and inhibition during stimulation at gamma and beta frequencies in the CA1 hippocampal region. *J. Neurophysiol.* **2001**, *85*, 2412–2422. [CrossRef]
6. Isomura, Y.; Sugimoto, M.; Fujiwara-Tsukamoto, Y.; Yamamoto-Muraki, S.; Yamada, J.; Fukuda, A. Synaptically activated Cl^- accumulation responsible for depolarizing GABAergic responses in mature hippocampal neurons. *J. Neurophysiol.* **2003**, *90*, 2752–2756. [CrossRef]
7. Jedlicka, P.; Deller, T.; Gutkin, B.S.; Backus, K.H. Activity-Dependent Intracellular Chloride Accumulation and Diffusion Controls GABA(A) Receptor-Mediated Synaptic Transmission. *Hippocampus* **2011**, *21*, 885–898.
8. Lillis, K.P.; Kramer, M.A.; Mertz, J.; Staley, K.J.; White, J.A. Pyramidal cells accumulate chloride at seizure onset. *Neurobiol. Dis.* **2012**, *47*, 358–366. [CrossRef]
9. Sato, S.S.; Artoni, P.; Landi, S.; Cozzolino, O.; Parra, R.; Pracucci, E.; Trovato, F.; Szczurkowska, J.; Luin, S.; Arosio, D.; et al. Simultaneous two-photon imaging of intracellular chloride concentration and pH in mouse pyramidal neurons in vivo. *Proc. Natl. Acad. Sci. USA* **2017**, *114*, E8770–E8779. [CrossRef]
10. Raimondo, J.V.; Markram, H.; Akerman, C.J. Short-term ionic plasticity at GABAergic synapses. *Front. Synaptic Neurosci.* **2012**, *4*, 5. [CrossRef]
11. Kaila, K.; Price, T.J.; Payne, J.A.; Puskarjov, M.; Voipio, J. Cation-chloride cotransporters in neuronal development, plasticity and disease. *Nat. Rev. Neurosci.* **2014**, *15*, 637–654. [CrossRef] [PubMed]
12. Staley, K.J.; Proctor, W.R. Modulation of mammalian dendritic $GABA_A$ receptor function by the kinetics of Cl^- and HCO_3^- transport. *J. Physiol.* **1999**, *519*, 693–712. [CrossRef] [PubMed]
13. Jedlicka, P.; Backus, K.H. Inhibitory transmission, activity-dependent ionic changes and neuronal network oscillations. *Physiol. Res.* **2006**, *55*, 139–149. [PubMed]
14. Wright, R.; Raimondo, J.V.; Akerman, C.J. Spatial and Temporal Dynamics in the Ionic Driving Force for GABA(A) Receptors. *Neural Plast.* **2011**, 278395. [CrossRef]
15. Doyon, N.; Prescott, S.A.; Castonguay, A.; Godin, A.G.; Kroger, H.; De Koninck, Y. Efficacy of Synaptic Inhibition Depends on Multiple, Dynamically Interacting Mechanisms Implicated in Chloride Homeostasis. *PLoS Comput. Biol.* **2011**, *7*, 9. [CrossRef]
16. Mohapatra, N.; Tonnesen, J.; Vlachos, A.; Kuner, T.; Deller, T.; Nagerl, U.V.; Santamaria, F.; Jedlicka, P. Spines slow down dendritic chloride diffusion and affect short-term ionic plasticity of GABAergic inhibition. *Sci. Rep.* **2016**, *6*, 23196. [CrossRef] [PubMed]
17. Buchin, A.; Chizhov, A.; Huberfeld, G.; Miles, R.; Gutkin, B.S. Reduced Efficacy of the KCC2 Cotransporter Promotes Epileptic Oscillations in a Subiculum Network Model. *J. Neurosci.* **2016**, *36*, 11619–11633. [CrossRef] [PubMed]
18. Staley, K.J.; Soldo, B.L.; Proctor, W.R. Ionic mechanisms of neuronal excitation by inhibitory GABAA receptors. *Science* **1995**, *269*, 977–981. [CrossRef]
19. Sun, M.K.; Zhao, W.Q.; Nelson, T.J.; Alkon, D.L. Theta rhythm of hippocampal CA1 neuron activity: Gating by GABAergic synaptic depolarization. *J. Neurophysiol.* **2001**, *85*, 269–279. [CrossRef]
20. Doyon, N.; Vinay, L.; Prescott, S.A.; De Koninck, Y. Chloride Regulation: A Dynamic Equilibrium Crucial for Synaptic Inhibition. *Neuron* **2016**, *89*, 1157–1172. [CrossRef]
21. Thompson, S.M.; Gähwiler, B.H. Activity-dependent disinhibition. I. Repetitive stimulation reduces IPSP driving force and conductance in the hippocampus in vitro. *J. Neurophysiol.* **1989**, *61*, 501–511. [CrossRef]
22. Doyon, N.; Prescott, S.A.; De Koninck, Y. Mild KCC2 Hypofunction Causes Inconspicuous Chloride Dysregulation that Degrades Neural Coding. *Front. Cell. Neurosci.* **2016**, *9*, 516. [CrossRef]
23. Bernard, C.; Cossart, R.; Hirsch, J.C.; Esclapez, M.; Ben Ari, Y. What is GABAergic inhibition? How is it modified in epilepsy? *Epilepsia* **2000**, *41*, S90–S95. [CrossRef]
24. Birke, G.; Draguhn, A. No Simple Brake—The Complex Functions of Inhibitory Synapses. *Pharmacopsychiatry* **2010**, *43*, S21–S31. [CrossRef]
25. Ben-Ari, Y.; Cherubini, E.; Corradetti, R.; Gaiarsa, J.-L. Giant synaptic potentials in immature rat CA3 hippocampal neurones. *J. Physiol.* **1989**, *416*, 303–325. [CrossRef]
26. Luhmann, H.J.; Prince, D.A. Postnatal maturation of the GABAergic system in rat neocortex. *J. Neurophysiol.* **1991**, *65*, 247–263. [CrossRef]
27. Owens, D.F.; Boyce, L.H.; Davis, M.B.; Kriegstein, A.R. Excitatory GABA responses in embryonic and neonatal cortical slices demonstrated by gramicidin perforated-patch recordings and calcium imaging. *J. Neurosci.* **1996**, *16*, 6414–6423. [CrossRef]

28. Hanganu, I.L.; Kilb, W.; Luhmann, H.J. Functional Synaptic Projections onto Subplate Neurons in Neonatal Rat Somatosensory Cortex. *J. Neurosci.* **2002**, *22*, 7165–7176. [CrossRef]
29. Achilles, K.; Okabe, A.; Ikeda, M.; Shimizu-Okabe, C.; Yamada, J.; Fukuda, A.; Luhmann, H.J.; Kilb, W. Kinetic properties of Cl uptake mediated by Na^+-dependent K^+-$2Cl^-$ cotransport in immature rat neocortical neurons. *J. Neurosci.* **2007**, *27*, 8616–8627. [CrossRef]
30. Kirmse, K.; Kummer, M.; Kovalchuk, Y.; Witte, O.W.; Garaschuk, O.; Holthoff, K. GABA depolarizes immature neurons and inhibits network activity in the neonatal neocortex in vivo. *Nat. Commun.* **2015**, *6*, 7750. [CrossRef]
31. Rohrbough, J.; Spitzer, N.C. Regulation of intracellular Cl^- levels by Na(+)-dependent Cl^- cotransport distinguishes depolarizing from hyperpolarizing GABAA receptor-mediated responses in spinal neurons. *J. Neurosci.* **1996**, *16*, 82–91. [CrossRef] [PubMed]
32. Yamada, J.; Okabe, A.; Toyoda, H.; Kilb, W.; Luhmann, H.J.; Fukuda, A. Cl^- uptake promoting depolarizing GABA actions in immature rat neocortical neurones is mediated by NKCC1. *J. Physiol.* **2004**, *557*, 829–841. [CrossRef] [PubMed]
33. Valeeva, G.; Tressard, T.; Mukhtarov, M.; Baude, A.; Khazipov, R. An Optogenetic Approach for Investigation of Excitatory and Inhibitory Network GABA Actions in Mice Expressing Channelrhodopsin-2 in GABAergic Neurons. *J. Neurosci.* **2016**, *36*, 5961–5973. [CrossRef] [PubMed]
34. Kolbaev, S.N.; Achilles, K.; Luhmann, H.J.; Kilb, W. Effect of depolarizing GABA(A)-mediated membrane responses on excitability of Cajal-Retzius cells in the immature rat neocortex. *J. Neurophysiol.* **2011**, *106*, 2034–2044. [CrossRef] [PubMed]
35. Owens, D.F.; Kriegstein, A.R. Is there more to GABA than synaptic inhibition? *Nat. Rev. Neurosci.* **2002**, *3*, 715–727. [CrossRef] [PubMed]
36. Ben Ari, Y.; Khalilov, I.; Kahle, K.T.; Cherubini, E. The GABA Excitatory/Inhibitory Shift in Brain Maturation and Neurological Disorders. *Neuroscientist* **2012**, *18*, 467–486. [CrossRef] [PubMed]
37. Luhmann, H.J.; Kirischuk, S.; Sinning, A.; Kilb, W. Early GABAergic circuitry in the cerebral cortex. *Curr. Opin. Neurobiol.* **2014**, *26*, 72–78. [CrossRef]
38. Sipila, S.T.; Huttu, K.; Soltesz, I.; Voipio, J.; Kaila, K. Depolarizing GABA acts on intrinsically bursting pyramidal neurons to drive giant depolarizing potentials in the immature hippocampus. *J. Neurosci.* **2005**, *25*, 5280–5289. [CrossRef] [PubMed]
39. Allene, C.; Cattani, A.; Ackman, J.B.; Bonifazi, P.; Aniksztejn, L.; Ben Ari, Y.; Cossart, R. Sequential Generation of Two Distinct Synapse-Driven Network Patterns in Developing Neocortex. *J. Neurosci.* **2008**, *28*, 12851–12863. [CrossRef]
40. Chub, N.; O'Donovan, M.J. Post-episode depression of GABAergic transmission in spinal neurons of the chick embryo. *J. Neurophysiol.* **2001**, *85*, 2166–2176. [CrossRef]
41. Lindsly, C.; Gonzalez-Islas, C.; Wenner, P. Activity Blockade and GABA(A) Receptor Blockade Produce Synaptic Scaling through Chloride Accumulation in Embryonic Spinal Motoneurons and Interneurons. *PLoS ONE* **2014**, *9*, e94559. [CrossRef] [PubMed]
42. Kolbaev, S.N.; Luhmann, H.J.; Kilb, W. Activity-dependent scaling of GABAergic excitation by dynamic Cl^- changes in Cajal-Retzius cells. *Pflugers Arch.* **2011**, *461*, 557–565. [CrossRef] [PubMed]
43. Gonzalez-Islas, C.; Chub, N.; Garcia-Bereguiain, M.A.; Wenner, P. GABAergic synaptic scaling in embryonic motoneurons is mediated by a shift in the chloride reversal potential. *J. Neurosci.* **2010**, *30*, 13016–13020. [CrossRef]
44. Khalilov, I.; Minlebaev, M.; Mukhtarov, M.; Khazipov, R. Dynamic Changes from Depolarizing to Hyperpolarizing GABAergic Actions during Giant Depolarizing Potentials in the Neonatal Rat Hippocampus. *J. Neurosci.* **2015**, *35*, 12635–12642. [CrossRef] [PubMed]
45. Lombardi, A.; Jedlicka, P.; Luhmann, H.J.; Kilb, W. Giant Depolarizing Potentials Trigger Transient Changes in the Intracellular Cl^- Concentration in CA3 Pyramidal Neurons of the Immature Mouse Hippocampus. *Front. Cell. Neurosci.* **2018**, *12*, 420. [CrossRef]
46. Kowalski, J.; Gan, J.; Jonas, P.; Pernia-Andrade, A.J. Intrinsic membrane properties determine hippocampal differential firing pattern in vivo in anesthetized rats. *Hippocampus* **2016**, *26*, 668–682. [CrossRef]
47. Behrens, C.J.; Ul Haq, R.; Liotta, A.; Anderson, M.L.; Heinemann, U. Nonspecific effects of the gap junction blocker mefloquine on fast hippocampal network oscillations in the adult rat in vitro. *Neuroscience* **2011**, *192*, 11–19. [CrossRef] [PubMed]

48. Bormann, J.; Hamill, O.P.; Sakmann, B. Mechanism of anion permeation through channels gated by glycine and gamma-aminobutyric acid in mouse cultured spinal neurones. *J. Physiol.* **1987**, *385*, 243–286. [CrossRef]
49. Fatima-Shad, K.; Barry, P.H. Anion Permeation in GABA- and Glycine-Gated Channels of Mammalian Cultured Hippocampal Neurons. *Proc. Biol. Sci.* **1993**, *253*, 69–75.
50. Ruusuvuori, E.; Li, H.; Huttu, K.; Palva, J.M.; Smirnov, S.; Rivera, C.; Kaila, K.; Voipio, J. Carbonic Anhydrase Isoform VII Acts as a Molecular Switch in the Development of Synchronous Gamma-Frequency Firing of Hippocampal CA1 Pyramidal Cells. *J. Neurosci.* **2004**, *24*, 2699–2707. [CrossRef]
51. Kaila, K.; Voipio, J. Postsynaptic fall in intracellular pH induced by GABA-activated bicarbonate conductance. *Nature* **1987**, *330*, 163–165. [CrossRef]
52. Wang, G.J.; Randall, R.D.; Thayer, S.A. Glutamate-Induced Intracellular Acidification of Cultured Hippocampal-Neurons Demonstrates Altered Energy-Metabolism Resulting from Ca^{2+} Loads. *J. Neurophysiol.* **1994**, *72*, 2563–2569. [CrossRef]
53. Kilb, W.; Schlue, W.R. Mechanism of the kainate-induced intracellular acidification in leech Retzius neurons. *Brain Res.* **1999**, *824*, 168–182. [CrossRef]
54. Qian, N.; Sejnowski, T.J. When Is an Inhibitory Synapse Effective. *Proc. Natl. Acad. Sci. USA* **1990**, *87*, 8145–8149. [CrossRef]
55. Kuner, T.; Augustine, G.J. A genetically encoded ratiometric indicator for chloride: Capturing chloride transients in cultured hippocampal neurons. *Neuron* **2000**, *27*, 447–459. [CrossRef]
56. Kaila, K.; Ruusuvuori, E.; Seja, P.; Voipio, J.; Puskarjov, M. GABA actions and ionic plasticity in epilepsy. *Curr. Opin. Neurobiol.* **2014**, *26*, 34–41. [CrossRef] [PubMed]
57. Lewin, N.; Aksay, E.; Clancy, C.E. Computational modeling reveals dendritic origins of GABA(a)-mediated excitation in ca1 pyramidal neurons. *PLoS ONE* **2012**, *7*, e47250. [CrossRef]
58. Dusterwald, K.M.; Currin, C.B.; Burman, R.J.; Akerman, C.J.; Kay, A.R.; Raimondo, J.V. Biophysical models reveal the relative importance of transporter proteins and impermeant anions in chloride homeostasis. *Elife* **2018**, *7*, e39575. [CrossRef]
59. Luhmann, H.J.; Reiprich, R.A.; Hanganu, I.; Kilb, W. Cellular physiology of the neonatal rat cerebral cortex: Intrinsic membrane properties, sodium and calcium currents. *J. Neurosci. Res.* **2000**, *62*, 574–584. [CrossRef]
60. Rheims, S.; Minlebaev, M.; Ivanov, A.; Represa, A.; Khazipov, R.; Holmes, G.L.; Ben-Ari, Y.; Zilberter, Y. Excitatory GABA in rodent developing neocortex in vitro. *J. Neurophysiol.* **2008**, *100*, 609–619. [CrossRef]
61. Ben-Ari, Y.; Woodin, M.A.; Sernagor, E.; Cancedda, L.; Vinay, L.; Rivera, C.; Legendre, P.; Luhmann, H.J.; Bordey, A.; Wenner, P.; et al. Refuting the challenges of the developmental shift of polarity of GABA actions: GABA more exciting than ever! *Front. Cell. Neurosci.* **2012**, *6*, 35. [CrossRef]
62. Kaila, K.; Lamsa, K.; Smirnov, S.; Taira, T.; Voipio, J. Long-lasting GABA-mediated depolarization evoked by high-frequency stimulation in pyramidal neurons of rat hippocampal slice is attributable to a network-driven, bicarbonate-dependent K^+ transient. *J. Neurosci.* **1997**, *17*, 7662–7672. [CrossRef] [PubMed]
63. Dallwig, R.; Deitmer, J.W.; Backus, K.H. On the mechanism of GABA-induced currents in cultured rat cortical neurons. *Pflugers Arch.* **1999**, *437*, 289–297. [CrossRef]
64. Sun, M.; Dahl, D.; Alkon, D.L. Heterosynaptic transformation of GABAergic gating in the hippocampus and effects of carbonic anhydrase inhibition. *J. Pharmacol. Exp. Ther.* **2001**, *296*, 811–817. [PubMed]
65. Rivera, C.; Voipio, J.; Kaila, K. Two developmental switches in GABAergic signalling: The K^+- Cl^- cotransporter KCC2 and carbonic anhydrase CAVII. *J. Physiol.* **2005**, *562*, 27–36. [CrossRef] [PubMed]
66. Earnhardt, J.N.; Qian, M.Z.; Tu, C.K.; Lakkis, M.M.; Bergenhem, N.C.H.; Laipis, P.J.; Tashian, R.E.; Silverman, D.N. The catalytic properties of murine carbonic anhydrase VII. *Biochemistry* **1998**, *37*, 10837–10845. [CrossRef] [PubMed]
67. Kaila, K. Ionic basis of $GABA_A$ receptor channel function in the nervous system. *Prog. Neurobiol.* **1994**, *42*, 489–537. [CrossRef]
68. Doischer, D.; Hosp, J.A.; Yanagawa, Y.; Obata, K.; Jonas, P.; Vida, I.; Bartos, M. Postnatal Differentiation of Basket Cells from Slow to Fast Signaling Devices. *J. Neurosci.* **2008**, *28*, 12956–12968. [CrossRef]
69. Kilb, W.; Luhmann, H.J. Spontaneous GABAergic postsynaptic currents in Cajal-Retzius cells in neonatal rat cerebral cortex. *Eur. J. Neurosci.* **2001**, *13*, 1387–1390. [CrossRef]
70. Kubota, Y. Untangling GABAergic wiring in the cortical microcircuit. *Curr. Opin. Neurobiol.* **2014**, *26*, 7–14. [CrossRef]

71. Misgeld, U.; Deisz, R.A.; Dodt, H.U.; Lux, H.D. The role of chloride transport in postsynaptic inhibition of hippocampal neurons. *Science* **1986**, *232*, 1413–1415. [CrossRef] [PubMed]
72. Gonzalez-Islas, C.; Chub, N.; Wenner, P. NKCC1 and AE3 appear to accumulate chloride in embryonic motoneurons. *J. Neurophysiol.* **2009**, *101*, 507–518. [CrossRef] [PubMed]
73. Kakazu, Y.; Uchida, S.; Nakagawa, T.; Akaike, N.; Nabekura, J. Reversibility and cation selectivity of the K^+-Cl^- cotransport in rat central neurons. *J. Neurophysiol.* **2000**, *84*, 281–288. [CrossRef] [PubMed]
74. Kahle, K.T.; Staley, K.J.; Nahed, B.V.; Gamba, G.; Hebert, S.C.; Lifton, R.P.; Mount, D.B. Roles of the cation-chloride cotransporters in neurological disease. *Nat. Clin. Pract. Neurol.* **2008**, *4*, 490–503. [CrossRef] [PubMed]
75. Khirug, S.; Ahmad, F.; Puskarjov, M.; Afzalov, R.; Kaila, K.; Blaesse, P. A single seizure episode leads to rapid functional activation of KCC2 in the neonatal rat hippocampus. *J. Neurosci.* **2010**, *30*, 12028–12035. [CrossRef] [PubMed]
76. Inoue, K.; Furukawa, T.; Kumada, T.; Yamada, J.; Wang, T.Y.; Inoue, R.; Fukuda, A. Taurine Inhibits K^+-Cl^- Cotransporter KCC2 to Regulate Embryonic Cl^- Homeostasis via With-no-lysine (WNK) Protein Kinase Signaling Pathway. *J. Biol. Chem.* **2012**, *287*, 20839–20850. [CrossRef]
77. Russell, J.M. Sodium-potassium-chloride cotransport. *Physiol. Rev.* **2000**, *80*, 211–276. [CrossRef] [PubMed]
78. Delpire, E.; Austin, T.M. Kinase regulation of Na^+-K^+-$2Cl^-$ cotransport in primary afferent neurons. *J. Physiol.* **2010**, *588*, 3365–3373. [CrossRef]
79. Bar-Yehuda, D.; Korngreen, A. Space-clamp problems when voltage clamping neurons expressing voltage-gated conductances. *J. Neurophysiol.* **2008**, *99*, 1127–1136. [CrossRef]
80. Backus, K.H.; Deitmer, J.W.; Friauf, E. Glycine-activated currents are changed by coincident membrane depolarization in developing rat auditory brainstem neurones. *J. Physiol.* **1998**, *507*, 783–794. [CrossRef]
81. Ellis, R.J.; Minton, A.P. Cell biology—Join the crowd. *Nature* **2003**, *425*, 27–28. [CrossRef] [PubMed]
82. McDougal, R.A.; Morse, T.M.; Carnevale, T.; Marenco, L.; Wang, R.; Migliore, M.; Miller, P.L.; Shepherd, G.M.; Hines, M.L. Twenty years of ModelDB and beyond: Building essential modeling tools for the future of neuroscience. *J. Comput. Neurosci.* **2017**, *42*, 1–10. [CrossRef] [PubMed]
83. Horikawa, K.; Armstrong, W.E. A versatile means of intracellular labeling: Injection of biocytin and its detection with avidin conjugates. *J. Neurosci. Meth.* **1988**, *25*, 1–11. [CrossRef]
84. Schröder, R.; Luhmann, H.J. Morphology, electrophysiology and pathophysiology of supragranular neurons in rat primary somatosensory cortex. *Eur. J. Neurosci.* **1997**, *9*, 163–176. [CrossRef] [PubMed]
85. De Schutter, E.; Smolen, P. Calcium Dynamics in Large Neuronal Models. In *Methods in Neuronal Modeling*; Koch, C., Segev, I., Eds.; MIT Press: Cambridge, MA, USA, 1998; pp. 211–250.
86. De Schutter, E. Modeling intracellular calcium dynamics. In *Computational Modeling Methods for Neuroscientists*; MIT Press: Cambridge, MA, USA, 2010; pp. 93–105.
87. Mohapatra, N.; Deans, H.; Santamaria, F.; Jedlicka, P. Modeling Ion Concentrations. In *Encyclopedia of Computational Neuroscience*; Jaeger, D., Jung, R., Eds.; Springer: New York, NY, USA, 2015. [CrossRef]
88. Hines, M.L.; Carnevale, N.T. Expanding NEURON's repertoire of mechanisms with NMODL. *Neural Comput.* **2000**, *12*, 995–1007. [CrossRef]
89. Santhakumar, V.; Aradi, I.; Soltesz, I. Role of mossy fiber sprouting and mossy cell loss in hyperexcitability: A network model of the dentate gyrus incorporating cell types and axonal topography. *J. Neurophysiol.* **2005**, *93*, 437–453. [CrossRef] [PubMed]
90. Ruusuvuori, E.; Kirilkin, I.; Pandya, N.; Kaila, K. Spontaneous network events driven by depolarizing GABA action in neonatal hippocampal slices are not attributable to deficient mitochondrial energy metabolism. *J. Neurosci.* **2010**, *30*, 15638–15642. [CrossRef]
91. Mitchell, R.A.; Herbert, D.A.; Carman, C.T. Acid-Base Constants and Temperature Coefficients for Cerebrospinal Fluid. *J. Appl. Physiol.* **1965**, *20*, 27–30. [CrossRef] [PubMed]